



Elp3-mediated codon-dependent translation promotes mTORC2 activation and regulates macrophage polarization

Dawei Chen^{1,2,3} , Ivan Nemazanyy⁴ , Olivier Peulen^{1,5} , Kateryna Shostak^{1,2,3}, Xinyi Xu^{1,2,3}, Seng Chuan Tang^{1,2,3}, Caroline Wathieu^{1,2,3} , Silvia Turchetto^{1,3,6}, Sylvia Tielens^{1,2,3}, Laurent Nguyen^{1,3,6} , Pierre Close^{1,3,7,8}, Christophe Desmet^{1,9}, Sebastian Klein¹⁰ , Alexandra Florin¹⁰, Reinhard Büttner¹⁰ , Georgios Petrellis¹¹ , Benjamin Dewals^{11,†} & Alain Chariot^{1,2,3,8,*}

Abstract

Macrophage polarization is a process whereby macrophages acquire distinct effector states (M1 or M2) to carry out multiple and sometimes opposite functions. We show here that translational reprogramming occurs during macrophage polarization and that this relies on the Elongator complex subunit Elp3, an enzyme that modifies the wobble uridine base U34 in cytosolic tRNAs. Elp3 expression is downregulated by classical M1-activating signals in myeloid cells, where it limits the production of pro-inflammatory cytokines via FoxO1 phosphorylation, and attenuates experimental colitis in mice. In contrast, alternative M2-activating signals upregulate Elp3 expression through a PI3K- and STAT6-dependent signaling pathway. The metabolic reprogramming linked to M2 macrophage polarization relies on Elp3 and the translation of multiple candidates, including the mitochondrial ribosome large subunit proteins Mrpl3, Mrpl13, and Mrpl47. By promoting translation of its activator Ric8b in a codon-dependent manner, Elp3 also regulates mTORC2 activation. Elp3 expression in myeloid cells further promotes Wnt-driven tumor initiation in the intestine by maintaining a pool of tumor-associated macrophages exhibiting M2 features. Collectively, our data establish a functional link between tRNA modifications, mTORC2 activation, and macrophage polarization.

Keywords Elp3; macrophage polarization; mitochondrial translation; mTORC2; tRNA modifications

Subject Categories Immunology; RNA Biology

DOI 10.15252/embj.2021109353 | Received 2 August 2021 | Revised 5 July 2022 | Accepted 7 July 2022 | Published online 3 August 2022

The EMBO Journal (2022) 41: e109353

Introduction

Macrophages are critical in homeostasis processes, in anti-microbial, and inflammatory activity in host defense as well as in the resolution of inflammation and wound healing (Murray & Wynn, 2011). Their response to microenvironmental cues allows them to acquire distinct effector states in order to carry out multiple functions. Their plasticity helps macrophages to acquire tailored activities within tissues and is often addressed through the concept of macrophage polarization (Pulendran & Artis, 2012; Murray *et al.*, 2014; Murray, 2017). Interferon- γ (IFN- γ) is the canonical type 1 cytokine which, together with bacterial lipopolysaccharide (LPS), is associated with a type 1 immune environment and triggers a proinflammatory profile that is referred to as “M1” or “classical” macrophage polarization. *In vivo*, macrophages with M1 characteristics secrete a variety of pro-inflammatory cytokines (TNF, IL-1 β , or IL-6) and cytotoxic molecules (reactive oxygen species and nitric oxide) to activate other immune cells and to carry out their microbicidal activity and anti-tumor immune responses (Murray *et al.*, 2014). In contrast, interleukin 4 (IL-4) and IL-13, which are cytokines typically associated with type 2 immune responses, trigger

1 Interdisciplinary Cluster for Applied Genoproteomics, University of Liege, Liege, Belgium

2 Laboratory of Medical Chemistry, University of Liege, Liege, Belgium

3 GIGA Stem Cells, University of Liege, Liege, Belgium

4 Platform for Metabolic Analyses, Structure Fédérative de Recherche Necker, INSERM US24/CNRS UMS 3633, Paris, France

5 Metastasis Research Laboratory (MRL), GIGA Cancer, University of Liege, Liège, Belgium

6 Laboratory of Molecular Regulation of Neurogenesis, University of Liege, Liege, Belgium

7 Laboratory of Cancer Signaling, University of Liege, Liege, Belgium

8 Walloon Excellence in Life Sciences and Biotechnology (WELBIO), Wavres, Belgium

9 Laboratory of Cellular and Molecular Immunology, GIGA-I³, University of Liege, Liège, Belgium

10 Institute for Pathology-University Hospital Cologne, Köln, Germany

11 Laboratory of Immunology-Vaccinology, Fundamental and Applied Research in Animals and Health (FARAH), University of Liege, Liège, Belgium

*Corresponding author. Tel: +32 (0) 4 366 24 72; E-mail: alain.chariot@uliege.be

†These authors contributed equally to this work

different responses in macrophages, resulting in what is often referred to as M2 macrophage polarization (Stein *et al*, 1992; Puledran & Artis, 2012; Murray *et al*, 2014). M2 macrophages downplay inflammation, promote tissue repair and remodeling through the secretion of anti-inflammatory cytokines (IL-10), scavenging receptors (mannose receptor) and a variety of remodeling factors (Gordon & Martinez, 2010). Processes linked to M2 macrophage *in vivo* are notably involved in tumor growth and metastasis, in the cellular response to helminth infections as well as in insulin sensitivity in adipocytes (Lumeng *et al*, 2007; Gordon & Martinez, 2010). This initial classification was based on *in vitro* studies but it is now increasingly clear that macrophages display a more dynamic and varied spectrum of activation states in between the two extreme M1 and M2 classes, yet mechanisms by which macrophage polarization is regulated at the level of mRNA translation is poorly understood.

Cellular metabolism has emerged as an important regulator of macrophage function as signals involved in macrophage polarization cause major changes in their metabolic program (Saha *et al*, 2017). M1 macrophage polarization is associated with enhanced glycolysis, defective tricarboxylic acid (TCA) cycle and mitochondrial oxidative phosphorylation (OXPHOS) while M2 macrophages rely on TCA cycle and OXPHOS for energy generation (Vats *et al*, 2006; Rodríguez-Prados *et al*, 2010; O'Neill, 2016; Saha *et al*, 2017; Ryan & O'Neill, 2020).

The mechanistic target of Rapamycin (mTOR), a serine/threonine protein kinase, acts as a nutrient/energy sensor which couples nutrient availability to metabolic processes and critically regulates macrophage polarization (Düvel *et al*, 2010; Howell & Manning, 2011; Laplante & Sabatini, 2012; Byles *et al*, 2013). mTOR is part of two distinct complexes, mTORC1 and mTORC2, each complex having specific functions in cell signaling and metabolism (Liu & Sabatini, 2020). Myeloid-specific deficiency of *Rictor*, a specific adaptor molecule of mTORC2, blocks M2 polarization and impairs the cellular response to helminth infection (Hallowell *et al*, 2017). *Rictor*-deficient myeloid cells induce M1 macrophage polarization, similarly to the genetic deletion of *Tsc1*, a negative regulator of mTORC1, and consequently produce more inflammatory cytokines in response to LPS (Byles *et al*, 2013; Festuccia *et al*, 2014). Therefore, mTORC2 activation, linked to metabolic reprogramming, is critical in M2 macrophage polarization (Huang *et al*, 2016).

RNA modifications, which are defined as post-transcriptional changes in the chemical composition of RNA molecules, contribute to translational reprogramming and are involved in immune responses (Shulman & Stern-Ginossar, 2020). The most prevalent modified base found on messenger RNAs (mRNAs), N⁶-methyladenosine (m⁶A), regulate the antiviral response, at least through the modulation of interferon mRNAs (Rubio *et al*, 2018; Winkler *et al*, 2019). Although the majority of RNA modifications are found in noncoding RNAs, including transfer RNAs (tRNAs) and ribosomal RNAs, their biological relevance in immune responses remains to be elucidated. Among tRNA-modifying enzymes which target the tRNA anticodon, Elongator and Cytosolic thiolase (Ctu)-1/2 complexes exclusively modify the wobble uridine (U₃₄) base in cytosolic tRNAs (El Yacoubi *et al*, 2012). Ctu1, but not the associated Ctu2, harbors the enzymatic activity (Dewez *et al*, 2008). Elongator (Elp1-Elp6) includes Elp3, the catalytic subunit and Elp1, the scaffold protein, and promotes the formation of ⁵-methoxycarbonylmethyl (mcm⁵) or ⁵-carbamoylmethyl (ncm⁵) side chains on U₃₄ while Ctu1/2 adds a ²-thioylation (s²) on U₃₄ in the

last step of this cascade. Only specific tRNAs (Arg^{UCU}, Lys^{UUU}, Gln^{UUG} and Glu^{UUC}) are targeted by both enzymes (El Yacoubi *et al*, 2012). In mice, *Elp3* deficiency impairs indirect neurogenesis and consequently leads to microcephaly, at least due to enhanced Atf4 levels (Laguesse *et al*, 2015). *Elp3* expression in epithelial cells promotes Wnt-driven tumor initiation in the intestine and breast cancer metastasis, at least by promoting the expression of Sox9 and DEK in a codon-dependent manner, respectively (Ladang *et al*, 2015; Delaunay *et al*, 2016). *Elp3* also promotes the acquired resistance to a B-RAF inhibitor in metastatic melanoma through HIF1 α translation (Rapino *et al*, 2017). Mechanistically, Elp1 is activated by phosphorylation through an mTORC2-dependent pathway in melanoma cells (Rapino *et al*, 2018). In yeast, TORC2 also activates Elongator in a phospho-dependent manner while Elongator promotes the translation of key components of TORC2 (Candiracci *et al*, 2019). Therefore, the link between mTORC2 and some tRNA modifications seems conserved throughout evolution.

We show here that *Elp3* deficiency in myeloid cells potentiates the production of pro-inflammatory cytokines upon LPS stimulation, at least through decreased FoxO1 phosphorylation. As a result, *Elp3* deficiency exacerbates intestinal damage in a model of dextran sulfate sodium (DSS)-driven colitis. On the other hand, *Elp3* deficiency blocks IL-4-dependent M2 macrophage polarization. Mechanistically, *Elp3* deficiency impairs mTORC2 activation. Ric8b, a non-canonical guanine nucleotide exchange factor (GEF) acting as a positive regulator of mTORC2 (Nagai *et al*, 2020), relies on *Elp3* to be properly translated in a codon-dependent manner. Both transcriptomic signature and metabolic reprogramming triggered by IL-4 is defective upon *Elp3* deficiency. *Elp3* supports mitochondrial functions in metabolic reprogramming during macrophage polarization, at least through the production of some mitochondrial ribosome large subunit proteins. Finally, *Elp3* deficiency in myeloid cells delays Wnt-driven tumor initiation in the intestine by altering the pool of tumor-associated macrophages (TAMs). Therefore, *Elp3* blocks M1 but favors M2 macrophage polarization. Collectively, our data establish a functional link between some tRNA modifications, mTORC2 activation, and macrophage polarization.

Results

Elp3 deficiency potentiates the differentiation into M1 macrophage

It is currently unknown whether Elongator regulates the polarization of monocytes into M1 or M2 macrophages. To address this issue, we first look at the expression of its subunits in macrophages undergoing M1 polarization. *Elp3* and *Elp1* expression at both mRNA and protein levels were downregulated by both LPS and IFN γ in mouse peritoneal macrophages (Fig EV1A and B). Of note, levels of *Elp5* remained stable during M1 polarization while both *Elp4* and *Elp6* decreased, mostly at late time points (Fig EV1B). Interestingly, the thiolase Ctu1, but not Ctu2, was also downregulated by both IFN γ and LPS at the protein level (Fig EV1B). Therefore, downregulation of these tRNA-modifying enzymes is observed in cells undergoing differentiation into M1 macrophages.

To assess whether Elongator regulates the polarization of monocytes into M1 macrophages, we first inactivated *Elp3* in myeloid

cells by breeding our *Elp3^{lox/lox}* strain (Ladang et al, 2015) with the LysM-CRE mouse to generate the so-called « *Elp3^{AMye}* » strain where *Elp3* expression is abolished in myeloid cells (Fig 1A). As expected, levels of mcm⁵S² U34 tRNA modifications quantified by Mass Spectrometry were decreased in myeloid cells lacking *Elp3* (Fig 1B). Consistently, the pool of thiolated tRNAs in BMDMs lacking *Elp3* decreased, as assessed by Northern blots using UUC, UUG, and UUU probes (Fig EV1C). Similar experiments were conducted with total RNAs from intestinal epithelial cells (IECs) lacking or not *Elp3* as controls (Fig EV1C). We next isolated Thioglycollate-elicited peritoneal macrophages from both *Elp3^{Control}* and *Elp3^{AMye}* strains and stimulated them *ex-vivo* with a combination of LPS and IFN γ to trigger M1 macrophage polarization. Akt phosphorylation on serine 473, a hallmark of mTORC2 activation, was defective upon *Elp3* deficiency (Fig 1C). Consistently, the LPS/IFN γ -dependent phosphorylation of NdrG1, a mTORC2 substrate, was also defective upon *Elp3* deficiency (Fig 1D). Consistent with a defective Akt activation without *Elp3*, FoxO1, an Akt substrate (Brunet et al, 1999), was not properly phosphorylated in response to both LPS and IFN γ upon loss of *Elp3* in peritoneal macrophages (Fig 1C). Therefore, mTORC2 activation relies on *Elp3* expression in Thioglycollate-elicited peritoneal macrophages.

Inactivation of *Rictor* causes an hyperinflammatory phenotype in response to LPS, at least due to a defective Akt-dependent FoxO1 phosphorylation (Brown et al, 2011). Therefore, we reasoned that the defective FoxO1 phosphorylation seen upon *Elp3* deficiency may lead to enhanced macrophage-driven inflammation in response to LPS and IFN γ . To test this hypothesis, we assessed mRNA levels of several pro-inflammatory cytokines upon stimulation with IFN γ , LPS, or with a combination of both. mRNA levels of IL-6, IL-1 β , and IL12p40 in peritoneal macrophages treated with LPS or with both LPS and IFN γ were significantly enhanced upon *Elp3* deficiency (Fig 1E). As *Ct2* act in the same enzymatic cascade as *Elp3* (El Yacoubi et al, 2012), we next explored whether *Ct2* and *Elp3* deficiencies induced a similar phenotype in M1 macrophage polarization. *Ct2* deficiency in bone marrow-derived macrophages

(BMDMs) also impaired LPS/IFN γ -dependent Akt phosphorylation on S473 and potentiated the production of pro-inflammatory cytokines such as IL-6 and IL-1 β upon stimulation with LPS/IFN γ (Fig 1F and G, respectively). Taken together, our data indicate that *Elp3*, and by extension U₃₄ tRNA modifications, negatively regulates M1 macrophage polarization.

Elp3 deficiency in myeloid cells exacerbates experimental colitis

Pro-inflammatory M1 polarization of macrophages contributes to intestinal damage in mouse models of experimental colitis. As *Elp3* limits M1 macrophage polarization, we reasoned that *Elp3* deficiency in myeloid cells would potentiate phenotypical parameters in a model of experimental colitis. To address this issue, we treated both *Elp3^{Control}* and *Elp3^{AMye}* strains for 6 continuous days with Dextran sulfate sodium (DSS), which erodes the single layer of intestinal epithelial cells and causes colitis in mice. The survival time was decreased upon *Elp3* deficiency in myeloid cells (Fig 2A). Moreover, the weight loss due to DSS administration was more pronounced in *Elp3^{AMye}* mice (Fig 2B). Importantly, colon length in *Elp3^{AMye}* mice was reduced, reflecting a more severe phenotype following *Elp3* deficiency (Fig 2C). Consistently, mRNA levels of a variety of pro-inflammatory cytokines were more elevated in *Elp3^{AMye}* mice as was the histological score upon treatment with DSS (Fig 2D and E, respectively). Moreover, the percentage of macrophages expressing M1 markers (iNOS⁺/CD68⁺ cells) in inflamed intestinal crypts was higher in *Elp3^{AMye}* than in *Elp3^{Control}* mice subjected to DSS (Fig 2F). In agreement with the notion that *Elp3* deficiency is linked to an increased inflammatory status, patients suffering from ulcerative colitis showed lower levels of both *Elp1* and *Elp3* (Fig 2G). Of note, *Elp3* deficiency in myeloid cells did not impact the architecture of intestinal crypts, nor on both colon length and levels of pro-inflammatory cytokines (Fig EV1D–F, respectively). Therefore, *Elp3* limits the inflammatory response in a model of experimental colitis, at least by blocking M1 macrophage polarization.

Figure 1. Elp3 negatively regulates M1 macrophage polarization.

- A Generation of myeloid cells genetically inactivated for *Elp3*. *Elp3* mRNA and protein levels were assessed by Real-Time PCR with extracts isolated from peritoneal macrophages of *Elp3^{Control}* and *Elp3^{AMye}* mice. mRNA levels in *Elp3^{Control}* mice were set to 1 and levels in other experimental conditions were relative to that after normalization with *Gapdh* mRNA levels ($n = 3$ mice; mean \pm SD, Student *t*-test, *** $P < 0.001$). An anti-*Elp3* western blot (WB) is also illustrated. The anti-*Gapdh* blot is shown for normalization purposes.
- B Myeloid cells lacking *Elp3* show decreased levels of mcm⁵S² U34 tRNA modifications. Multiple tRNA modifications in BMDMs from both *Elp3^{Control}* and *Elp3^{AMye}* mice were quantified by Mass Spectrometry (see [Methods](#) for details).
- C, D Defective mTORC2 signaling upon *Elp3* deficiency in myeloid cells. Peritoneal macrophages from *Elp3^{Control}* and *Elp3^{AMye}* mice were isolated and cultured *ex-vivo*. They were untreated or stimulated with a combination of LPS (100 ng/ml) and IFN γ (50 ng/ml) for the indicated periods of time and the resulting cell extracts were subjected to WB analyses.
- E Enhanced mRNA levels of pro-inflammatory cytokines upon *Elp3* inactivation in myeloid cells subjected to LPS or to both LPS and IFN γ stimulations. Peritoneal macrophage from *Elp3^{Control}* or *Elp3^{AMye}* mice were unstimulated (« Control ») or treated with IFN γ (50 ng/ml), LPS (100 ng/ml) or with both IFN γ and LPS for 24 h and the resulting mRNAs of the listed pro-inflammatory cytokines were assessed by Real Time PCR. mRNA levels in *Elp3^{Control}* mice were set to 1 and levels in other experimental conditions were relative to that after normalization with *Gapdh* mRNA levels ($n = 6$ mice; mean \pm SD, Student *t*-test, ** $P < 0.01$, * $P < 0.05$).
- F mTORC2 activation by M1 polarization signals relies on *Ct2*. Control and *Ct2*-depleted bone marrow-derived macrophages (BMDMs; siRNA-mediated depletions) were treated or not with IFN γ (50 ng/ml) and LPS (100 ng/ml) and the resulting cell extracts were subjected to WB analyses.
- G *Ct2* deficiency potentiates M1 macrophage polarization. Control and *Ct2*-depleted BMDMs were treated or not with IFN γ (50 ng/ml) and LPS (100 ng/ml) for 24 h and the resulting mRNAs of the listed pro-inflammatory cytokines were assessed by Real Time PCR. mRNA levels in control BMDMs were set to 1 and levels in other experimental conditions were relative to that after normalization with *Gapdh* mRNA levels. Experiments were conducted in triplicates (mean \pm SD, Student *t*-test, * $P < 0.05$, ** $P < 0.01$, *** $P < 0.001$).

Source data are available online for this figure.

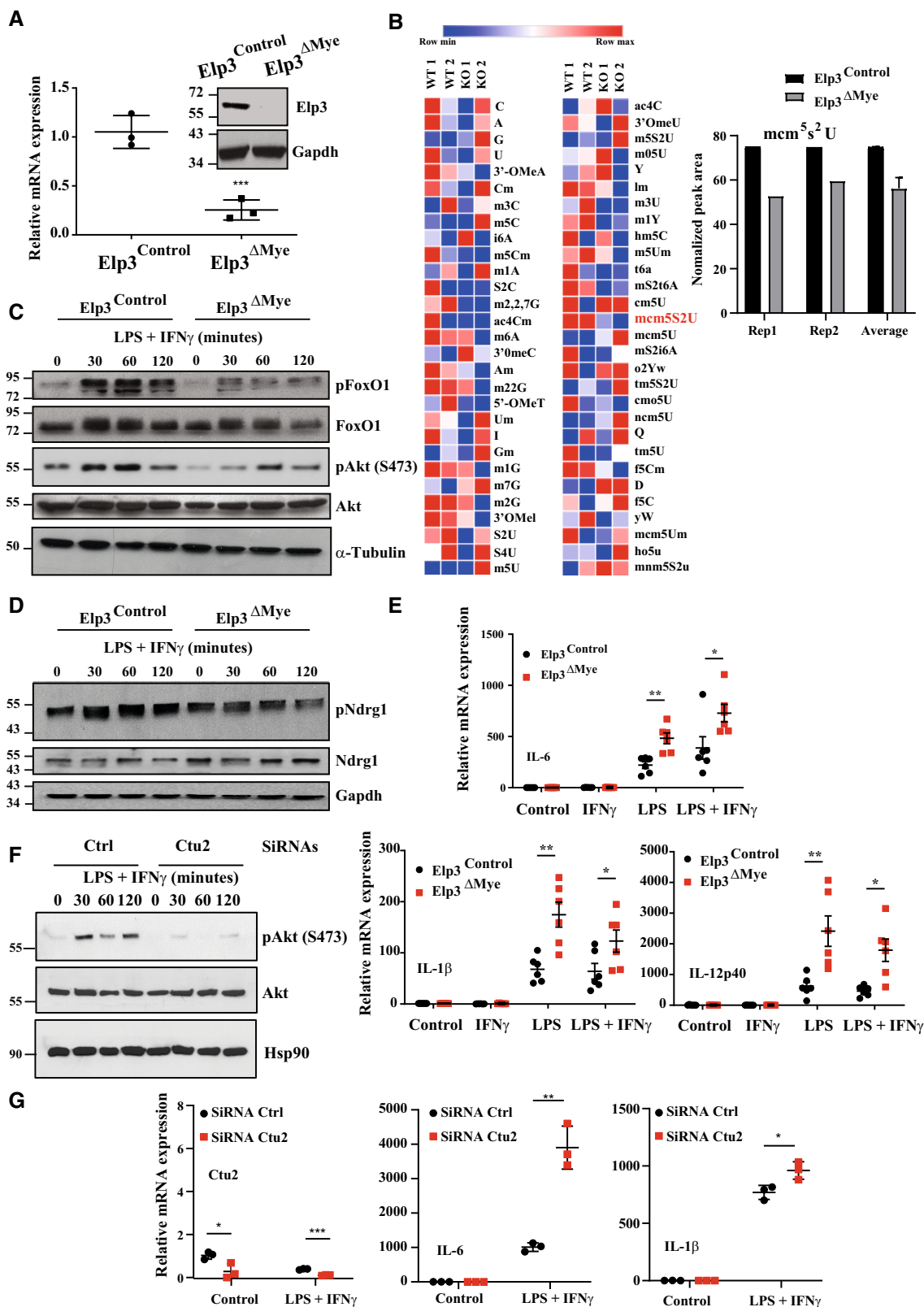


Figure 1.

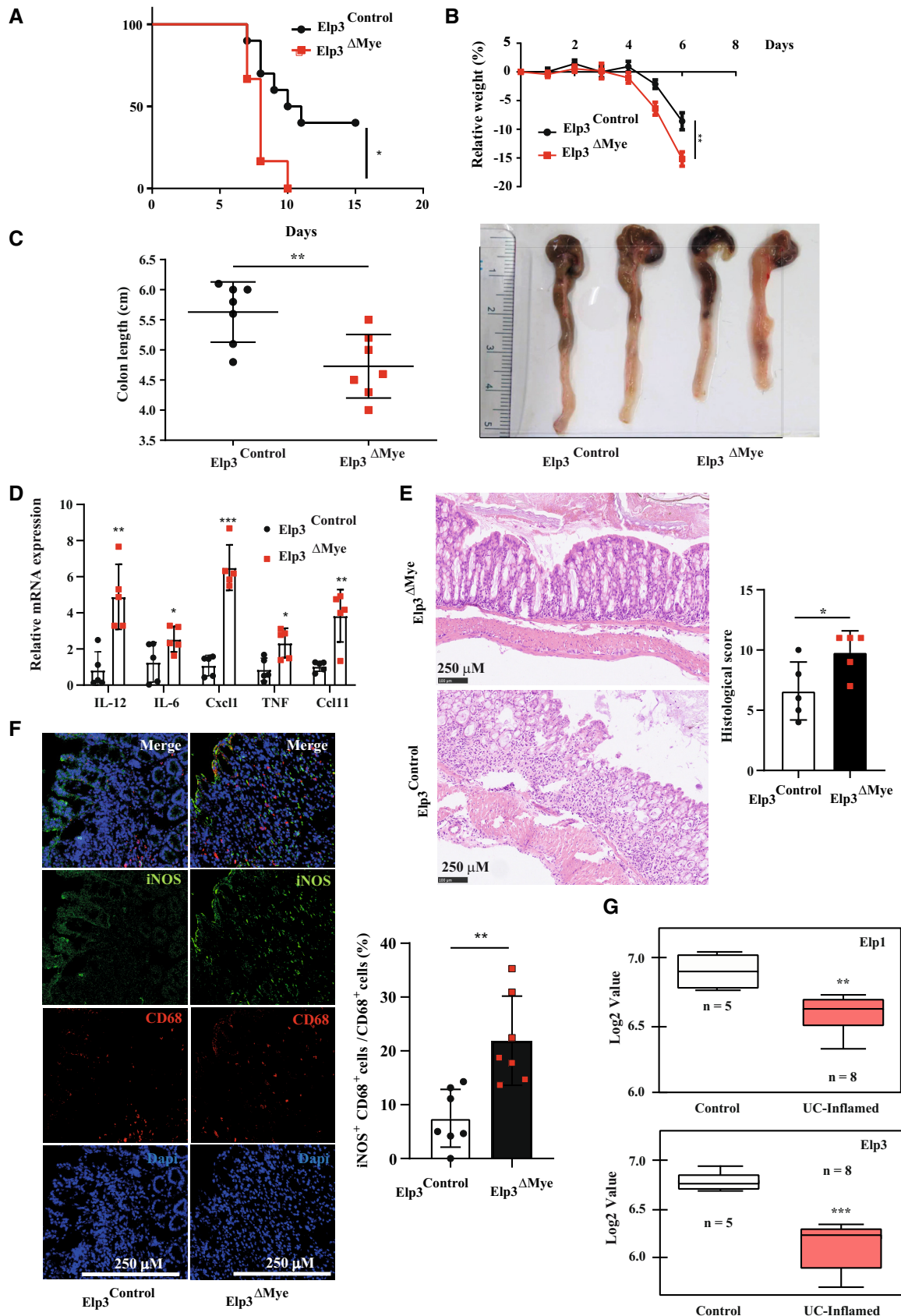


Figure 2.

Figure 2. Elp3 expression in myeloid cells protects from intestinal damage in an experimental model of colitis.

- A Decreased survival of mice lacking Elp3 expression in myeloid cells upon DSS administration ($n = 10$ mice per genotype; mean \pm SD, Student t -test, $*P < 0.05$).
- B, C Elp3 deficiency in myeloid cells exacerbates the weight loss and the decrease of colon length upon DSS administration ($n = 7$ mice; mean \pm SD, $**P < 0.01$).
- D Elp3 deficiency in myeloid cells potentiates the production of cytokines and chemokines upon DSS administration. mRNA levels of the indicated candidates in $Elp3^{Control}$ mice were set to 1 and levels in other experimental conditions were relative to that after normalization with Gapdh mRNA levels ($n = 5$ mice per genotype; mean \pm SD, Student t -test, $*P < 0.05$, $**P < 0.01$, $***P < 0.001$).
- E More severe histological score in mice lacking Elp3 in myeloid cells upon DSS administration. Representative intestinal crypts from the indicated genotypes are illustrated. The histological score was established as described in methods ($n = 5$ mice per genotype; mean \pm SD, Student t -test, $*P < 0.05$).
- F Increased infiltration of iNOS⁺/CD68⁺ cells upon DSS administration in $Elp3^{\Delta Mye}$ mice. The percentage of iNOS⁺ in CD68⁺ cells was established in both genotypes treated with DSS ($n = 7$ mice per genotype; mean \pm SD, Student t -test, $**P < 0.01$). Anti-iNOS and -CD68 immunofluorescence analyses carried out in intestinal crypts from both genotypes are illustrated.
- G Patients suffering from ulcerative colitis (UC) show reduced levels of both Elp1 and Elp3. The central band represents the mean value of relative expression in the investigated cohort. Boxes represent 75th and 25th percentile. Whiskers represent maximum and minimum values before the upper and lower fence, respectively ($**P < 0.01$, $***P < 0.001$; GSE9452-GEO DataSets, Definition of an ulcerative colitis preinflammatory state).

Source data are available online for this figure.

Elp3 expression is induced by IL-4 and IL-13 in macrophages

IL-4 and IL-13 trigger cell polarization into anti-inflammatory M2 macrophages. To assess whether Elp3 regulates M2 macrophage polarization, we first treated macrophages with IL-4, IL-13, or with both cytokines. These cytokines induced Elp3, Elp1, Ctu1, and Ctu2 mRNAs and protein levels in mouse peritoneal macrophages (Figs 3A and EV2A, respectively). Consistently, the pool of thiolated tRNAs increased upon IL-4/IL-13 induction in Thioglycollate-elicited peritoneal macrophages while this pool of chemically modified tRNAs decreased upon treatment with LPS/IFN γ (Fig 3B). Elp3 induction by both IL-4 and IL-13 occurred through a PI3K-dependent pathway as the PI3K inhibitor Wortmannin-blocked Elp3

induction by these cytokines in peritoneal macrophages (Fig 3C). Of note, Wortmannin had no effect on IL-4-dependent Elp3 induction at the mRNA level, indicating that its effect on Elp3 expression is post-transcriptional (Fig 3D). As mTOR is activated by IL-4 in macrophages (Byles *et al*, 2013), we next explored whether mTOR activation was required for Elp3 induction by IL-4. Rictor but not Raptor deficiency severely interfered with Elp3 expression in BMDMs, indicating that mTORC2 but not mTORC1 promotes Elp3 expression (Fig 3E). As the transcription factor Stat6 is also critical for gene induction by IL-4 (Hou *et al*, 1994), we next explored whether the pharmacological inhibition of Stat6 had any consequences on Elp3 expression. As expected, AS1517499 severely abolished Stat6 phosphorylation (Fig 3F). Moreover, this Stat6 inhibitor

Figure 3. Elp3 induction by IL-4 through multiple signaling pathways.

- A IL-4 and IL-13 induce the expression of tRNA-modifying enzymes in macrophages. Peritoneal macrophages were untreated (« Control ») or stimulated with IL-4 (10 ng/ml), IL-13 (10 ng/ml) or with both cytokines for 24 h and cell extracts from the resulting cells were subjected to WB analyses.
- B The pool of thiolated tRNAs in macrophages is enhanced by IL-4/IL-13 but decreased by LPS/IFN γ . On the left, Northern blot analysis assessing t:Q(UUG) tRNA thiolation in Thioglycollate-elicited peritoneal macrophages subjected to the indicated treatments for 24 h. On the right, quantification of t:Q(UUG) tRNA thiolation, calculated as the ration of thiolated over nonthiolated t:Q(UUG), in the indicated experimental conditions.
- C Elp3 induction by IL-4/IL-13 occurs through a PI3K-dependent pathway. Peritoneal macrophages were pretreated with DMSO (control vehicle) or with Wortmannin (200 nM) for 1 h and subsequently left untreated or stimulated with IL-4 (10 ng/ml)/IL-13 (10 ng/ml) for the indicated periods of time. Cell extracts from the resulting cells were subjected to WB analyses.
- D PI3K inhibition does not impact on Elp3 mRNA levels. Peritoneal macrophages were pretreated with DMSO (control vehicle) or with Wortmannin (200 nM) for 1 h and subsequently left untreated or stimulated with IL-4 (10 ng/ml) for 24 h. Elp3 mRNA levels were quantified in all experimental conditions by Real-Time PCR. Elp3 mRNA levels in unstimulated cells were set to 1 and levels in other experimental conditions were relative to that after normalization with Gapdh mRNA levels. Experiments were conducted in triplicates (mean \pm SD, Student t -test, $**P < 0.01$).
- E Rictor but not Raptor deficiency impairs Elp3 expression. BMDMs were transfected with the indicated siRNAs and the resulting cells were treated or not with IL-4 (10 ng/ml)/IL-13 (10 ng/ml) for 24 h. Cell extracts were subjected to WB analyses.
- F IL-4/IL-13 rely on Stat6 to induce Elp3 expression. Peritoneal macrophages were pretreated with the control vehicle (DMSO) or with the Stat6 pharmacological inhibitor AS1517499 (5 μ M) for 1 h and subsequently left unstimulated or treated with IL-4 (10 ng/ml)/IL-13 (10 ng/ml) for the indicated periods of time. Cell extracts from the resulting cells were subjected to WB analyses.
- G Stat6 is recruited on the *Elp3* promoter in an IL-4-dependent manner. CHIP assays using an anti-Stat6 antibody were conducted in RAW 264.7 cells to assess Stat6 recruitment on a Stat-DNA binding site found in the *Elp3* promoter. IgG antibody was used as a negative result. The histogram shows Stat6 recruitment on the Stat DNA-binding site with or without IL-4 (10 ng/ml) treatment for 2 h. Results obtained with four independent experiments (mean \pm SD, Student t -test, $*P < 0.05$) are illustrated.
- H–J Elp3 deficiency in myeloid cells impairs multiple signaling pathways triggered by IL-4 (H, I, and J), IL-13 (H) or by both cytokines (H). Peritoneal macrophages isolated from the indicated mouse genotypes were untreated or stimulated with IL-4 (10 ng/ml) (H, I, and J), IL-13 (10 ng/ml) (H) or with both cytokines (H) for 8 h (H) or for the indicated periods of time (I and J) and the resulting cell extracts were subjected to WB analyses.
- K Elp3 deficiency in BMDMs impairs the production of M2 markers upon stimulation with IL-4/IL-13. mRNAs of M2 markers were assessed by Real Time PCR. mRNA levels in unstimulated macrophages from $Elp3^{Control}$ mice were set to 1 and levels in other experimental conditions were relative to that after normalization with Gapdh mRNA levels ($n = 4$ mice; mean \pm SD, Student t -test, $*P < 0.05$, $***P < 0.001$).
- L Elp3 promotes M2 macrophage polarization. Peritoneal macrophages isolated from the indicated mouse genotypes were untreated or stimulated with IL-4/IL-13 (10 ng/ml) for 24 h and the resulting cell extracts were subjected to WB analyses.

Source data are available online for this figure.

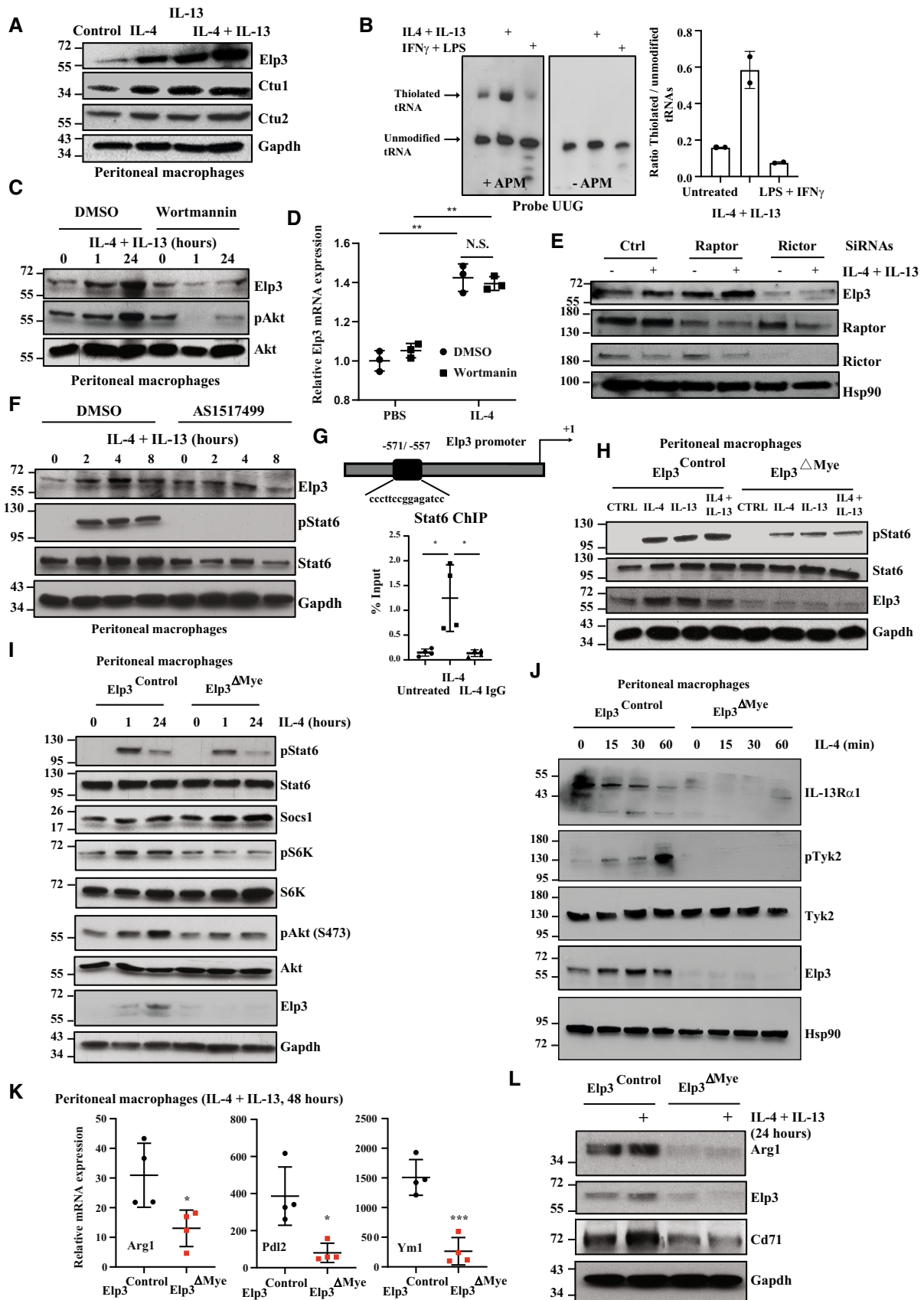


Figure 3.

also interfered with the induction of *Elp3* expression by IL-4 in peritoneal macrophages (Fig 3F). Consistently, Stat6 was also recruited on a Stat DNA-binding site in the *Elp3* promoter in an IL-4-dependent manner (Fig 3G). Therefore, IL-4 relies on both Stat6 and mTORC2 to induce *Elp3* expression in macrophages.

Elp3 promotes M2 macrophage polarization

Having established that IL-4/IL-13 induce *Elp3* expression, we next assessed whether loss of *Elp3* impairs M2 macrophage polarization. The genetic inactivation of *Elp3* in peritoneal macrophages impaired Stat6 phosphorylation upon stimulation with IL-4, IL-13 or with both cytokines (Fig 3H and I). Of note, protein levels of *Socs1*, a negative regulator of Stat signaling, were increased upon IL-4 stimulation in peritoneal macrophages from *Elp3^{ΔMye}* mice (Fig 3I). Moreover, IL-4-dependent S6K phosphorylation was also defective upon *Elp3* deficiency (Fig 3I). Importantly, mTORC2-dependent Akt phosphorylation on serine 473 was also impaired following *Elp3* deficiency (Fig 3I). Therefore, *Elp3* deficiency impairs multiple signaling pathways triggered by IL-4 in peritoneal macrophages. To learn more on molecular mechanisms by which *Elp3* promotes Stat6 activation upon IL-4 stimulation, we looked at early events occurring in this signaling pathway. Protein levels of IL-13R α 1 were decreased in peritoneal macrophages lacking *Elp3* expression (Fig 3J). Moreover, *Tyk2*, a JAK kinase family member, was not properly phosphorylated upon IL-4 stimulation in peritoneal macrophages lacking *Elp3*, indicating that very early events in IL-4 signaling are controlled by *Elp3* (Fig 3J). As IL-4 signaling is impaired upon *Elp3* deficiency, the expression of M2 markers such as arginase 1, *Cd71*, *Pdl2*, and *Ym1* was reduced in IL-4/IL-13-stimulated peritoneal macrophages from *Elp3^{ΔMye}* mice (Fig 3K and L). Consistently, *Ctu2* deficiency in BMDMs also impaired IL-4-dependent Akt phosphorylation on S473 and also impaired the production of M2 markers in IL-4-stimulated BMDMs (Fig EV2B and C, respectively).

To further explore the role of *Elp3* in M2 macrophage polarization, we conducted unbiased transcriptomic analyses (RNA-Seq) combined with Gene Set Enrichment analyses (GSEA) using BMDMs from *Elp3^{Control}* and *Elp3^{ΔMye}* mice treated or not with IL-4 *ex-vivo*

for 2 h. Genes normally induced through LPS-dependent pathways were upregulated upon *Elp3* deficiency, which fits with our data showing that *Elp3* deficiency potentiates M1 macrophage polarization (Fig 4A). Importantly, a Ppar γ -dependent signature was lost upon *Elp3* deficiency, which also fits with our data demonstrating that M2 macrophage polarization relies on *Elp3* (Fig 4A). Consistently, the induction of Ppar γ by IL-4/IL-13 was abolished in peritoneal macrophages lacking *Elp3* (Fig 4B). Dozens of mRNAs whose expression is induced by IL-4 and linked to M2 macrophage polarization were actually not properly induced in IL-4-stimulated BMDMs lacking *Elp3* (Fig 4C). Interestingly, *Irf4*, which acts downstream of mTORC2 to promote M2 macrophage polarization (Huang *et al*, 2016), was not properly expressed upon *Elp3* deficiency in peritoneal macrophages (Fig 4D). Besides these top 50 genes whose expression was impaired upon IL-4 treatment in BMDMs lacking *Elp3*, we also identified 806 less expressed genes as well as 416 genes whose expression increased in IL-4-induced BMDMs from *Elp3^{ΔMye}* mice compared to BMDMs from *Elp3^{Control}* mice (Fig 4E). To study the consequences of *Elp3* deficiency on the proteome of macrophages undergoing M2 polarization, we performed an integrated comparative proteomic analysis of *Elp3^{Control}* and *Elp3^{ΔMye}* BMDMs treated with IL-4 for 4 h. Correlation analyses of RNA-seq and proteomic data showed that 139 proteins were significantly downregulated in BMDMs from *Elp3^{ΔMye}* mice, while corresponding mRNAs did not change (Fig 4F). Interestingly, many of these proteins showed a clear prominent mRNA use of codons Lys^{AAA}, Gln^{CAA}, and Glu^{GAA} known to rely on *Elp3* to be translated (Fig 4G). Collectively, our data demonstrate that *Elp3* is a key enzyme involved in M2 macrophage polarization.

Metabolic reprogramming linked to M2 macrophage polarization requires Elp3

As macrophage polarization is intrinsically linked to metabolic reprogramming, we next investigated whether *Elp3* deficiency had any impact on metabolic remodeling. Extracts from peritoneal macrophages of *Elp3^{Control}* and *Elp3^{ΔMye}* mice treated or not with IL-4 *ex-vivo* were subjected to mass spectrometry analyses in order to

Figure 4. The transcriptomic reprogramming during M2 macrophage polarization relies on Elp3.

- Elp3* deficiency potentiates the expression of genes induced by LPS-dependent pathways and impairs a Ppar γ -dependent transcriptional signature. The figure shows some GSEA analyses carried out on RNA-Seq data done with total RNAs of BMDMs from *Elp3^{Control}* and *Elp3^{ΔMye}* mice treated with IL-4 *ex-vivo*.
- Defective induction of Ppar γ by IL-4/IL-13 upon *Elp3* deficiency. Cell extracts from peritoneal macrophages of *Elp3^{Control}* and *Elp3^{ΔMye}* mice treated or not with IL-4/IL-13 were subjected to WB analyses.
- Elp3* deficiency impairs the IL-4-dependent transcriptional signature. Cell extracts from BMDMs of *Elp3^{Control}* and *Elp3^{ΔMye}* mice treated or not with IL-4 for 2 h were subjected to RNA-Seq experiments. A heatmap is illustrated to show the defective induction of 50 genes by IL-4 upon *Elp3* deficiency.
- Defective *Irf4* expression upon IL-4 stimulation in peritoneal macrophages lacking *Elp3* expression. *Irf4* mRNA levels in peritoneal macrophages from untreated *Elp3^{Control}* mice were set to 1 and levels in other experimental conditions were relative to that after normalization with *Gapdh* mRNA levels ($n = 3$ mice; mean \pm SD, Student *t*-test, $**P < 0.01$).
- The IL-4-dependent transcriptomic signature requires *Elp3*. A volcano plot illustrating changes in mRNA levels in IL-4-stimulated BMDMs (2 h) from *Elp3^{Control}* and *Elp3^{ΔMye}* mice is shown.
- Identification of candidates whose protein but not mRNA levels are decreased in IL-4-treated BMDMs lacking *Elp3*. A volcano plot of correlation between changes in protein and mRNA levels is illustrated. Protein were extracted from BMDMs of *Elp3^{Control}* and *Elp3^{ΔMye}* mice treated for 4 h with IL-4. Red dots indicate candidates whose protein but not mRNA levels were downregulated in BMDMs from *Elp3^{ΔMye}* mice compared to BMDMs from *Elp3^{Control}* mice.
- Identification of candidates enriched in Lys^{AAA}, Gln^{CAA}, and Glu^{GAA} codons whose expression decreases in BMDMs lacking *Elp3*. A heatmap of the top 40 genes enriched in these codons is illustrated.

Source data are available online for this figure.

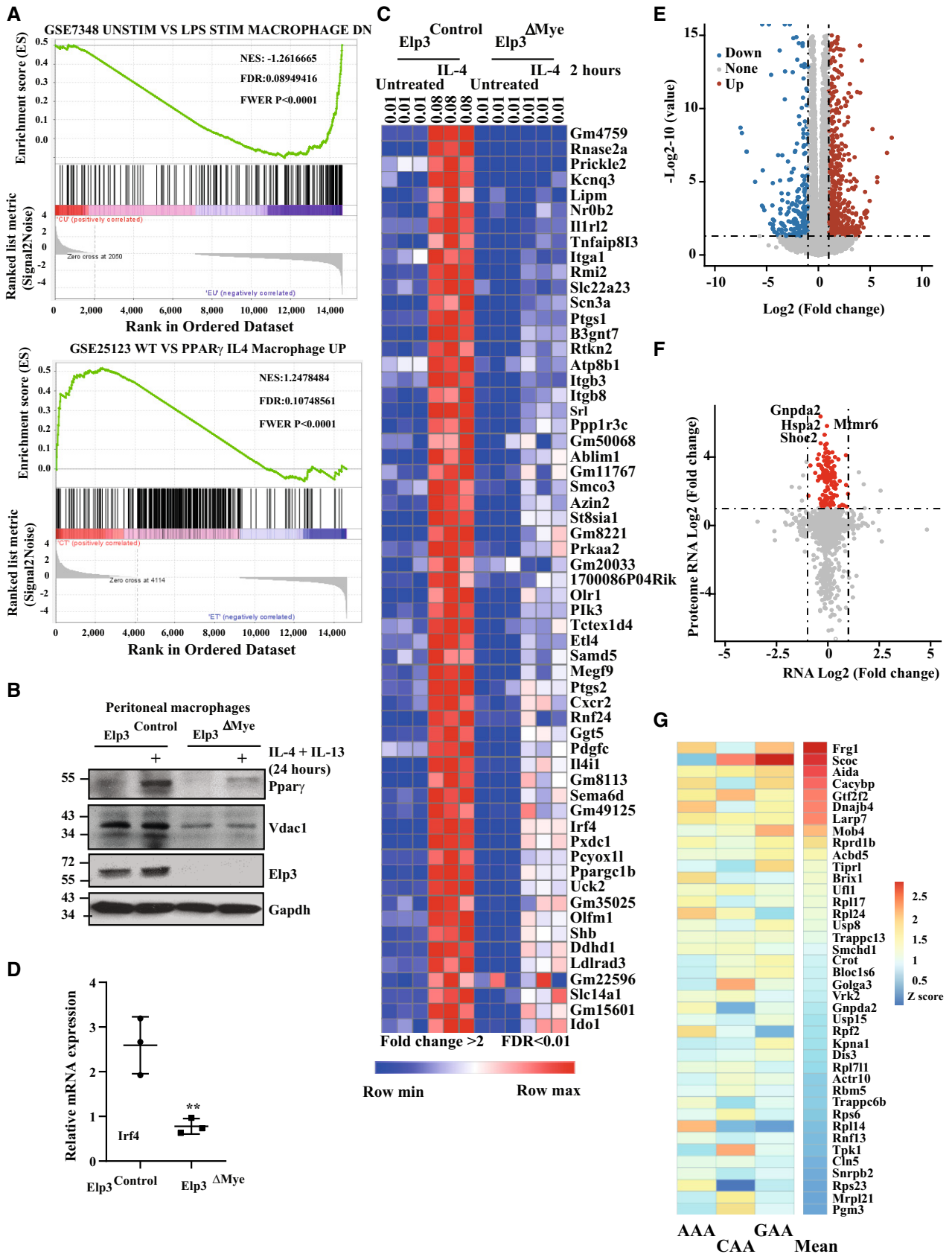


Figure 4.

establish their metabolic profile. In agreement with the fact that M2 macrophages rely on TCA cycle for glucose metabolism and energy generation (O'Neill, 2016) and in agreement with our data showing that *Elp3* deficiency impairs M2 macrophage polarization, TCA metabolites (malate, fumarate) accumulated in IL-4-stimulated peritoneal macrophages lacking *Elp3* expression, which reflects a defective TCA cycle (Figs 5A and EV3). This conclusion was raised through an enrichment overview of our metabolomic data (Fig 5B). Glutamine metabolism is another feature of M2 macrophages (Jha et al, 2015). In this context, α -ketoglutarate, which is produced via glutaminolysis, is essential for M2 macrophage polarization (Liu et al, 2017). Interestingly, α -ketoglutarate levels were decreased in IL-4-stimulated peritoneal macrophages from *Elp3*^{ΔMye} mice, suggesting that glutaminolysis is impaired without *Elp3* (Fig EV3). Moreover, glucose consumption has been reported to be elevated in M2 macrophages (Huang et al, 2016). Consistent with a defective M2 polarization without *Elp3*, glucose consumption was indeed impaired in macrophages from *Elp3*^{ΔMye} mice (Fig 5C). The use of glucose for UDP-GlcNAc synthesis is another metabolic feature of M2 macrophages (Jha et al, 2015). UDP-GlcNAc levels were down-regulated upon *Elp3* deficiency in IL-4-stimulated peritoneal macrophages (Fig 5A). Therefore, several metabolic pathways involved in M2 macrophage polarization, critically rely on *Elp3*.

To learn more on molecular mechanisms by which *Elp3* controls glucose consumption in macrophages, we looked at expression level of *Glut1*, a glucose transporter and found that *Glut1* mRNA levels were severely decreased in peritoneal macrophages from *Elp3*^{ΔMye} mice (Fig 5D). As the rate of conversion of glucose into pyruvate, a key step of glycolysis, accelerates the net rate of glucose consumption, we next looked at expression levels of platelet phosphofruktokinase (*Pfkfb*) and noticed a severely decreased expression upon *Elp3* deficiency as were mRNA levels of glucose phosphate isomerase (*Gpi1*; Fig 5D). Therefore, *Elp3* controls glucose consumption in macrophages, at least by promoting the expression of glucose transporter and enzymes involved in glycolysis.

Elp3 controls mitochondrial function in macrophages

A defective TCA cycle observed upon *Elp3* deficiency suggests that some mitochondrial functions may be disrupted. We indeed noticed that peritoneal macrophages lacking *Elp3* showed a reduced

mitochondrial complex I activity (Fig 5E). We also observed that the mitochondrial membrane potential in peritoneal macrophages from *Elp3*^{ΔMye} mice was impaired, as evidenced by FACS using potential-sensitive tetramethylrhodamine methyl ester (TMRM) fluorescence (Fig 5F). We next explored whether *Elp3* regulates mitochondrial oxidative phosphorylation based on the oxygen consumption rate (OCR), a measure of electron transport chain activity. Maximal but not basal OCR was significantly decreased in peritoneal macrophages from *Elp3*^{ΔMye} mice (Fig 5G). Consistently, the spare OCR capacity was decreased upon *Elp3* deficiency in peritoneal macrophages (Fig 5G). Collectively, our data indicate that *Elp3* expression is required for mitochondrial functions in peritoneal macrophages.

Elp3 promotes M2 macrophage polarization in vivo

To further assess whether M2 macrophage polarization requires *Elp3* *in vivo*, mice were administered with recombinant IL-4 complexed with anti-IL-4 monoclonal antibody (IL-4c) to extend the bioactive half-life of IL-4 *in vivo* and the expression of M2 markers (*arginase 1*, *Ucp1*, and *Ym1*) were quantified. Levels of these M2 markers were severely impaired in *Elp3*^{ΔMye} mice (Fig 6A). The i.p injection of IL-4c also elicits the robust proliferation of resident macrophages in the pleural and peritoneal cavity (Jenkins et al, 2011). These peritoneal macrophages (PMs) have been classified into two groups, referred to as large peritoneal macrophages (LPMs), which are resident macrophages and small peritoneal macrophages (SPMs), derived from bone marrow, according to their morphology (Cassado et al, 2015). Interestingly, loss of *Elp3* impaired IL-4c-induced LPM numbers but did not change the number of SPMs (Fig 6B and C, respectively). To address whether the lack of amplification of LPMs in IL-4c-treated *Elp3*^{ΔMye} mice was due to impaired proliferation, we stained peritoneal cells from both *Elp3*^{Control} and *Elp3*^{ΔMye} mice for Ki67 and EdU, two markers of cycling cells. *Elp3* deficiency decreased the number of both Ki67⁺ LPMs and EdU⁺ PMs (Fig 6D and E, respectively). To further characterize this cell proliferation defect in macrophages lacking *Elp3*, GSEA analyses for Hallmark gene sets were conducted and showed prominent enrichment of gene sets related to proliferation, including the mitotic spindle, G2/M checkpoint, and E2F targets gene sets, in our RNA-Seq data from IL-4 treated *Elp3*^{Control} and *Elp3*^{ΔMye} BMDMs

Figure 5. The transcriptomic reprogramming during M2 macrophage polarization relies on Elp3.

- A *Elp3* deficiency impairs levels of TCA cycle metabolites in IL-4-stimulated peritoneal macrophages. Peritoneal macrophages from *Elp3*^{Control} and *Elp3*^{ΔMye} mice (*n* = 3 per genotype) were treated with IL-4 for 24 h *ex-vivo* and the resulting extracts were subjected to Mass Spec analyses to extensively quantify metabolites.
- B *Elp3* deficiency is linked to a defective TCA cycle in peritoneal macrophages. Enrichment analyses carried out on our metabolomics data are illustrated.
- C *Elp3* controls glucose consumption in peritoneal macrophages. The glucose consumption rate was measured in peritoneal macrophages from *Elp3*^{Control} and *Elp3*^{ΔMye} mice (see Methods for details; *n* = 3 mice per genotype; mean ± SD, Student *t*-test, **P* < 0.05).
- D *Elp3* deficiency in peritoneal macrophages impairs the expression of enzymes involved in glucose consumption. mRNA levels of the indicated candidates in peritoneal macrophages from *Elp3*^{Control} mice were set to 1 and levels in *Elp3*^{ΔMye} mice were relative to that after normalization with *Gapdh* mRNA levels (*n* = 3 mice per genotype; mean ± SD, Student *t*-test, ****P* < 0.001, ***P* < 0.01, **P* < 0.05).
- E, F *Elp3* deficiency in peritoneal macrophages impairs mitochondrial complex I activity (E) and the mitochondrial membrane potential (F). Extracts from peritoneal macrophages of *Elp3*^{Control} and *Elp3*^{ΔMye} mice were used to assess complex I activity (E) (*n* = 3 mice per genotype; mean ± SD, Student *t*-test, **P* < 0.05). The mitochondrial membrane potential was assessed by FACS analyses by following-up TMRM (*n* = 3 mice per genotype; mean ± SD, Student *t*-test, ****P* < 0.001). Representative FACS panels are illustrated on the right.
- G *Elp3* expression in peritoneal macrophages is required for mitochondrial oxidative phosphorylation. Both basal and maximal oxygen consumption rate (OCR) as well as the spare OCR were measured with extracts from peritoneal macrophages of both *Elp3*^{Control} and *Elp3*^{ΔMye} mice (see Methods for details; *n* = 3 mice per genotype; mean ± SD, Student *t*-test, ****P* < 0.001, ***P* < 0.01).

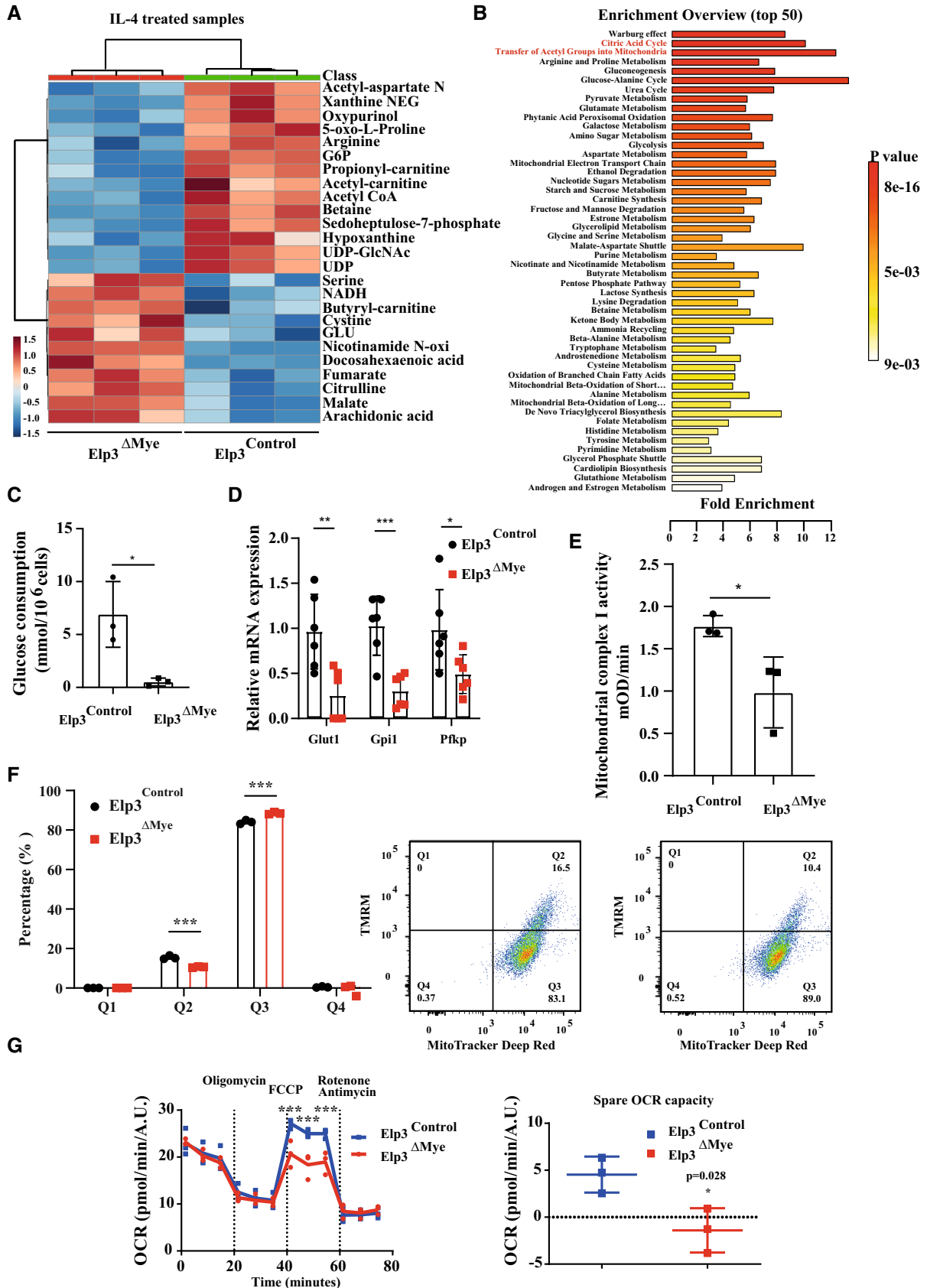


Figure 5.

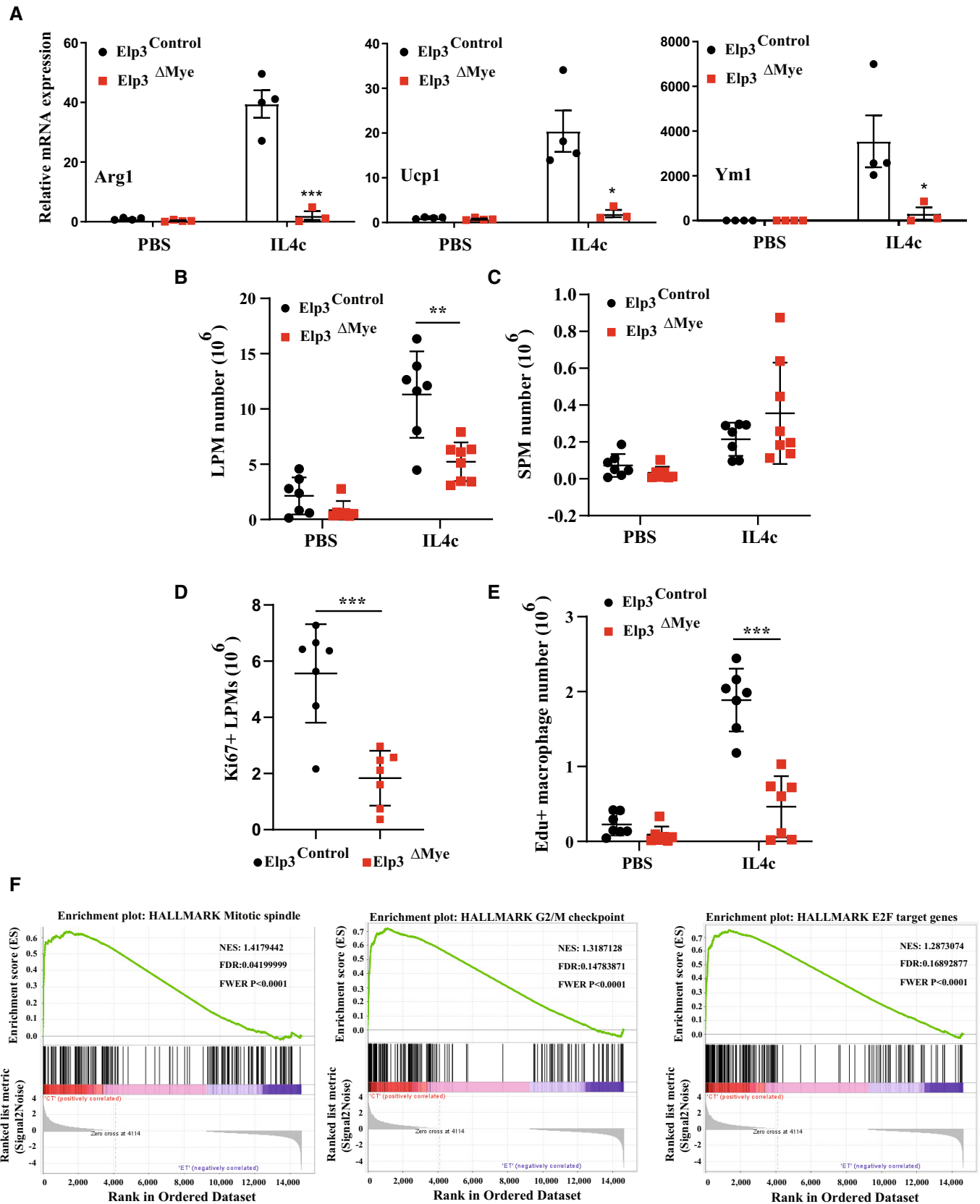


Figure 6.

Figure 6. Elp3 promotes M2 macrophage polarization *in vivo*.

- A Impaired production of M2 markers upon IL-4 activation *in vivo* in mice lacking *Elp3* in peritoneal macrophages. Mice of the indicated genotypes were treated with PBS or stimulated with IL-4 complex (IL-4c) and mRNA levels of the indicated candidates were assessed by Real Time PCR in the peritoneal exudate cells 4 days after the stimulation. mRNA levels in peritoneal exudate cells from untreated *Elp3*^{Control} mice were set to 1 and levels in other experimental conditions were relative to that after normalization with *Gapdh* mRNA levels ($n = 4$ mice; mean \pm SD, Student *t*-test, *** $P < 0.001$, ** $P < 0.01$, * $P < 0.05$).
- B Decreased number of large peritoneal macrophages (LPMs) lacking *Elp3* during M2 polarization. Numbers of LPMs (CD115⁺, ICAM2⁺, MHCII^{low}) sorted from *Elp3*^{Control} and *Elp3*^{AMye} mice treated by IL-4c are plotted (representative of two experiments, $n = 7$ mice per group, mean \pm SD, Student *t*-test, ** $P < 0.01$).
- C *Elp3* deficiency does not impact cell proliferation of small peritoneal macrophages upon IL-4c stimulation. Numbers of SPMs (CD115⁺, ICAM2⁺, MHC II^{high}) sorted from *Elp3*^{Control} and *Elp3*^{AMye} mice treated by IL-4c are plotted and data are illustrated as in B. (representative of two experiments, $n = 7$ per group, mean \pm SD, Student *t*-test, nonsignificant).
- D Decreased number of cycling LPMs lacking *Elp3* upon stimulation with IL-4c. Numbers of Ki67⁺ LPMs sorted from *Elp3*^{Control} and *Elp3*^{AMye} mice treated by IL-4c are plotted (representative of two experiments, $n = 7$ mice per group, mean \pm SD, Student *t*-test, *** $P < 0.001$).
- E Decreased number of Edu⁺ PM cells lacking *Elp3* upon stimulation with IL-4c. Numbers of Edu⁺ CD11⁺ cells sorted from *Elp3*^{Control} and *Elp3*^{AMye} mice treated by IL-4c are plotted (representative of two experiments, $n = 7$ per group, mean \pm SD, Student *t*-test, *** $P < 0.001$).
- F *Elp3* controls the proliferation of macrophages undergoing M2 polarization. GSEA analyses with gene expression RNA-seq data are illustrated. Representative Hallmarks enriched in *Elp3*^{Control} versus *Elp3*^{AMye} BMDMs treated by IL-4 for 2 h are shown.

(Fig 6F). Therefore, *Elp3* promotes M2 macrophage polarization *in vivo*, at least by supporting macrophage proliferation upon stimulation with IL-4c.

Elp3 promotes Ric8b expression in myeloid cells

As *Elp3* and mTORC2 deficiencies share overlapping phenotypes (Hallowell et al, 2017), we next looked for any positive regulator of mTORC2 activation whose translation may require *Elp3*. In this context, we got interested in Ric8b, a noncanonical guanine nucleotide exchange factor (GEF) whose deficiency impairs Akt phosphorylation on Serine 473 (Nagai et al, 2020). Ric8b mRNA levels were induced by IL-4 in BMDMs from both *Elp3*^{Control} and *Elp3*^{AMye} mice, suggesting that *Elp3* does not control Ric8b transcription (Fig EV4A). Importantly, Ric8b protein levels were also increased by IL-4 in BMDMs from *Elp3*^{Control} but not from *Elp3*^{AMye} mice, suggesting that *Elp3* may control Ric8b mRNA translation (Fig 7A). This conclusion was further supported by the fact that the induction of *Elp3* and Ric8b expression by IL-4 followed similar kinetics (Fig 7A). To explore whether *Elp3* promotes Ric8b mRNA translation, we carried out a Puro-PLA assay to detect newly synthesized Ric8b proteins in IL-4-stimulated BMDMs from both *Elp3*^{Control} and

Elp3^{AMye} mice. Interestingly, *Elp3* deficiency interfered with the production of Ric8b proteins, suggesting that Ric8b is one candidate whose mRNA translation is regulated by *Elp3*-dependent tRNA modifications (Fig 7B). As *Elp3* controls mRNA translation in a codon-dependent manner (Bauer et al, 2012), we generated a Ric8b mutant in which Lys^{AAA}, Gln^{CAA}, and Glu^{GAA} codons known to rely on *Elp3* to be properly decoded (“Ric8b WT”) where replaced by their cognate synonymous Lys^{AAG}, Gln^{CAG}, and Glu^{GAG} codons which do not require the U34 mcm⁵s² for their translation (“Ric8b MUT”; Fig 7C). While *Elp3* deficiency in BMDMs interfered with the production of Ric8b WT, Ric8b MUT was properly expressed in macrophages lacking *Elp3* (Fig 7C). Collectively, our data define Ric8b as a direct target of *Elp3* in macrophages. We next depleted Ric8b in BMDMs and assessed the consequences on IL-4-dependent mTORC2 activation. Ric8b-depleted BMDMs did not properly phosphorylate Akt and Ndr1 upon IL-4 stimulation, indicating that mTORC2 activation indeed relies on Ric8b (Fig 7D and E, respectively). Of note, Ric8b deficiency also impaired mTORC2 activation by LPS/IFN γ , as judged by a defective Akt and Ndr1 phosphorylation (Fig EV4B). As IL-4-dependent signaling was defective upon Ric8b deficiency, the production of M2 markers was also impaired in BMDMs lacking Ric8b upon stimulation with IL-4/IL-13 (Fig 7F and G). Similarly to *Elp3*

Figure 7. Elp3 promotes Ric8b expression.

- A The induction of Ric8b expression by IL-4 relies on *Elp3*. BMDMs from the indicated genotypes were treated or not with IL-4 (10 ng/ml) up to 24 h and the resulting cell extracts were subjected to WB analyses.
- B *Elp3* promotes Ric8b mRNA translation. BMDMs from *Elp3*^{Control} and *Elp3*^{AMye} mice were treated by IL-4 for 24 h, followed by a treatment with 10 μ g/ml puromycin for 5 min. To detect newly synthesized Ric8b proteins, a Puro-PLA assay was conducted. Representative images detecting Ric8b (Red) and α -Tubulin⁺ microtubules (green) in BMDMs are illustrated. On the right, the graph shows a quantification of signals for Ric8b in α -Tubulin⁺ areas. A random of six different areas were counted (6 technical replicates, mean \pm SD, Student's *t*-test, * $P < 0.05$).
- C Ric8b is a direct target of *Elp3*. BMDMs from *Elp3*^{Control} and *Elp3*^{AMye} mice were infected with a lentiviral GFP construct (negative control), Flag-Ric8b WT or with Flag-Ric8b MUT, as indicated and the resulting protein extracts were subjected to WB analyses to assess Ric8b and *Elp3* protein levels. *Gapdh* was used as a loading control.
- D, E Ric8b promotes IL-4-dependent mTORC2 activation. Control or Ric8b-depleted BMDMs were treated or not with IL-4 (10 ng/ml) for the indicated periods of time and the resulting cell extracts were subjected to WB analyses.
- F, G Ric8b deficiency impairs the production of M2 markers upon IL-4/IL-13 stimulation. Control or Ric8b-depleted BMDMs were stimulated or not with IL-4/IL-13 (10 ng/ml) for 24 h and the resulting RNAs were subjected to Real-Time PCR analyses. mRNA levels of the indicated candidates in control and unstimulated BMDMs were set to 1 and levels in other experimental conditions were relative to that after normalization with *Gapdh* mRNA levels ($n = 3$ mice per genotype; mean \pm SD, Student *t*-test, *** $P < 0.001$, ** $P < 0.01$).
- H Ric8b controls glucose consumption in BMDMs. The glucose consumption rate was measured in BMDMs transfected with a siRNA CTRL or Ric8b. Data from three biological replicates (3 mice per group) are shown (mean \pm SD, Student *t*-test, ** $P < 0.01$).

Source data are available online for this figure.

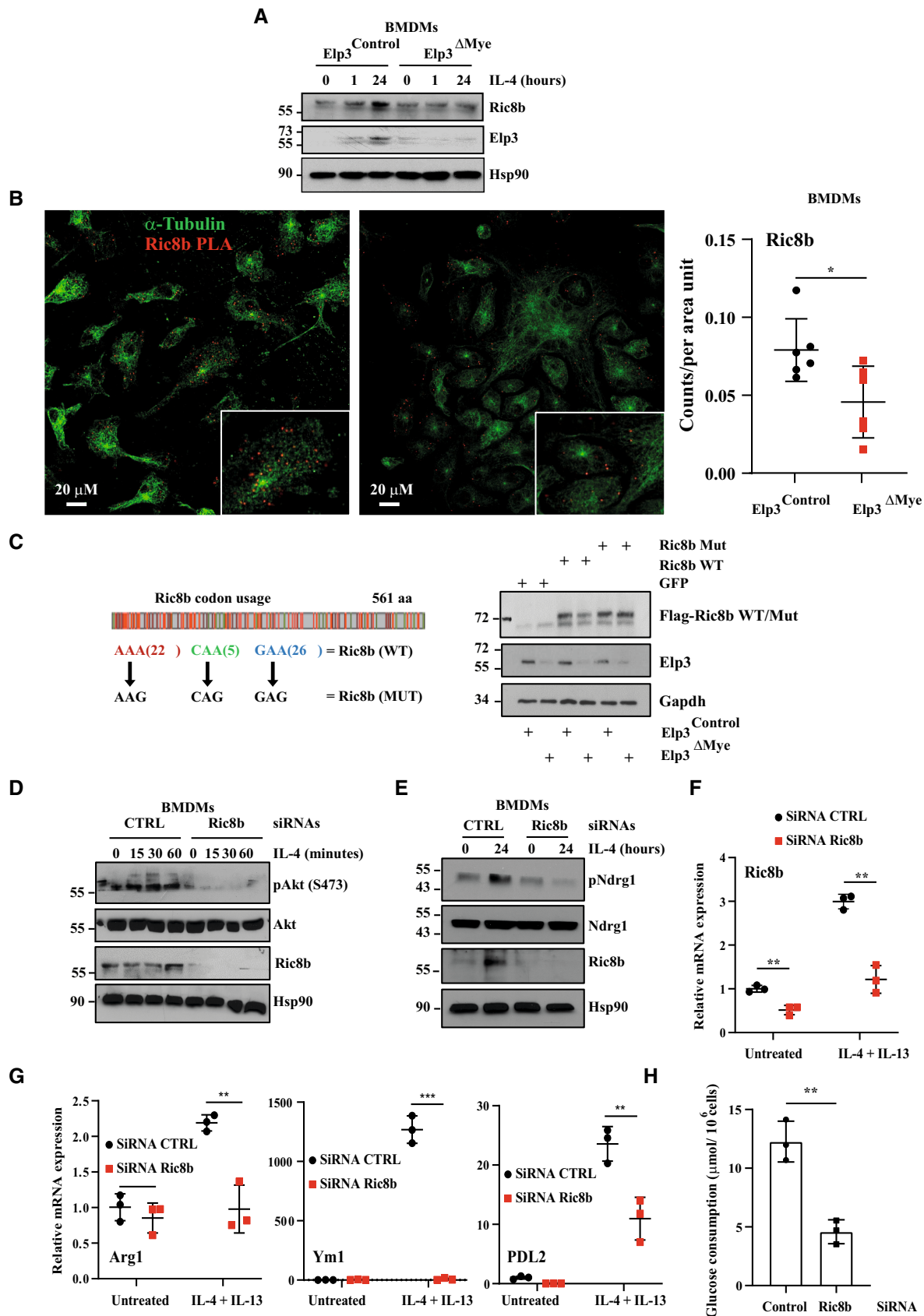


Figure 7.

deficiency, glucose consumption was also defective in IL-4/IL-13-stimulated BMDMs lacking Ric8b (Fig 7H). Collectively, these data indicate that Elp3 promotes mTORC2 signaling, at least through Ric8b in BMDMs.

Elp3 promotes the expression of some mitochondrial ribosome large subunit proteins

Having demonstrated that Elp3 is critical for mitochondrial functions in metabolic reprogramming linked to macrophage polarization, we next explored the underlying molecular mechanisms. *Elp3* deficiency leads to the accumulation of multiple proteins in aggregates, both in yeast and in mammalian cells (Nedialkova & Leidel, 2015; Rapino et al, 2018; Tavares et al, 2020). Likewise, *Elp3* deficiency caused the accumulation of protein candidates in aggregates from IL-4-stimulated BMDMs (Fig EV4C). We next isolated aggregates of BMDMs from both *Elp3*^{Control} and *Elp3*^{ΔMye} mice and subjected them to electrophoresis followed by Mass Spectrometry analysis (Fig EV4D). One thousand eight hundred and eight proteins were more expressed in aggregates upon IL-4 stimulation and levels of 623 candidates were more elevated upon *Elp3* deficiency in IL-4-stimulated BMDMs (Fig EV4E and F). Therefore, we focused our attention on 206 candidates whose expression was both induced by IL-4 and elevated upon *Elp3* deficiency in aggregates. We first subjected this proteomic signature to a Reactome analysis and highlighted a link with mitochondrial translation (Fig 8A). Interestingly, this signature included several mitochondrial ribosome large subunit proteins (Mrpl) showing an enrichment in Lys^{AAA}, Gln^{CAA}, and Glu^{GAA} codons known to rely on Elp3 to be decoded (Bauer et al, 2012; Fig 8B). We conducted western blot analysis using total extracts and found that both Mrpl3 and Mrpl13 levels were induced by IL-4/IL-13 in BMDMs (Fig 8C). Interestingly, protein levels of these mitochondrial candidates were similarly decreased upon IL-4/IL-13 stimulation in both BMDMs and PMs lacking Elp3 expression (Figs 8C and EV4G). Elp3 controls the expression of Mrpl3, Mrpl13, and Mrpl47 at a post-transcriptional level as mRNA levels of these candidates were similar in BMDMs from both *Elp3*^{Control} and *Elp3*^{ΔMye} mice (Fig EV4H). These results suggest that mitoribosomes may not be fully functional upon *Elp3* deficiency, with important consequences for mitochondrial translation. In agreement with this hypothesis, we found that protein levels of Mitochondrially Encoded Cytochrome C Oxidase III (Mt-co3) were severely decreased in both BMDMs and PMs lacking Elp3 (Figs 8C and EVI, respectively). Importantly, levels of Succinate dehydrogenase complex, subunit A (Sdha), a mitochondrial enzyme produced from nuclear DNA, were not defective in macrophages lacking Elp3 (Fig 8C). Therefore, *Elp3* deficiency causes defects in mitochondrial translation, at least by impairing levels and consequently functions of mitochondrial ribosomes. Importantly, Elp3 promotes M2 polarization, at least through the production of Mrpl13 as Mrpl13 deficiency in BMDMs also impaired the production of M2 markers upon stimulation with IL-4 (Fig 8D). Collectively, our data demonstrate that the production of some mitochondrial candidates is one mechanism by which Elp3 promotes M2 macrophage polarization.

Lack of Elp3 in peritoneal macrophages does not stabilize Atf4

Elp3 deficiency in T cells or in the hematopoietic system causes Atf4 stabilization (Lemaitre et al, 2021; Rosu et al, 2021). Although

stabilized ATF4 promotes rather than inhibit M2 macrophage polarization (Kim et al, 2018), we nevertheless addressed ATF4 expression in peritoneal macrophages lacking Elp3 expression. In contrast to T cells, Atf4 was not stabilized upon *Elp3* deficiency (Fig EV5A). Instead, Atf4 protein levels were decreased, especially after IL-4/IL-13 treatment (Fig EV5A). Consistently, mRNA levels of Atf4 target genes were not increased in IL-4-stimulated peritoneal macrophages lacking Elp3 expression (Fig EV5B). Collectively, these results indicate that *Elp3* deficiency does not stabilize Atf4 in peritoneal macrophages.

Elp3 expression in macrophages promotes Wnt-driven tumor development in the intestine

Intestinal tumors are infiltrated by TAMs, a class of macrophages with M2 features that positively regulates tumor development (Galdiero et al, 2013). As Elp3 controls M2 macrophage polarization, we next assessed whether *Elp3* deficiency in myeloid cells had any consequences on Wnt-driven tumor development in the intestine. To achieve this goal, we crossed *Elp3*^{Control} and *Elp3*^{ΔMye} mice with the *Apc*^{+/^{Min}} strain which spontaneously develop intestinal adenomas due to constitutive Wnt signaling (Su et al, 1992). The genetic inactivation of *Elp3* in myeloid cells extended mice survival in *Apc*^{+/^{Min}} mice (Fig 9A). *Apc*^{+/^{Min}} *Elp3*^{ΔMye} mice showed less adenomas in proximal, middle, and distal parts of the intestine than *Apc*^{+/^{Min}} *Elp3*^{Control} mice (Fig 9B). Moreover, splenomegaly, a typical feature observed in *Apc*^{+/^{Min}} mice, was less pronounced in *Apc*^{+/^{Min}} *Elp3*^{ΔMye} mice (Fig 9C). Importantly, the number of TAMs, defined as CD301⁺/F4/80⁺ cells among F4/80⁺ cells was decreased in *Apc*^{+/^{Min}} *Elp3*^{ΔMye} mice (Fig 9D). Therefore, *Elp3* deficiency in myeloid cells delays tumor development upon constitutive Wnt signaling, at least by negatively impacting on the pool of TAMs.

Discussion

We defined here tRNA-modifying enzymes Elp3 and Ctu2 as candidates that limit M1 and promote M2 macrophage polarization. We also demonstrate that Elp3 expression in myeloid cells is required in Wnt-driven tumor development in the intestine, at least by maintaining the pool of infiltrated M2-like macrophages in intestinal tumors. Mechanistically, we defined Ric8b and multiple IL-4-induced candidates including some mitochondrial proteins, as candidates whose production relies on Elp3. Therefore, our data indicate that U₃₄ tRNA-modifications critically regulate the biology of macrophages.

Macrophage polarization involves a dynamic regulation in the expression of tRNA-modifying enzymes such as Elp1/3 and Ctu1/2. Indeed, Elp3 expression is induced by IL-4 in macrophages but repressed by IFN γ . As a result, the pool of U₃₄ chemically modified tRNAs similarly change during macrophage polarization in order to control the translational reprogramming occurring during this process. We showed that Stat6 is recruited on the *Elp3* promoter to drive its expression upon stimulation by IL-4. Moreover, Rictor also promotes Elp3 induction by IL-4, possibly through the mTORC2-dependent phosphorylation of transcription factors recruited on the *Elp3* promoter. Therefore, Elp3 expression is regulated by multiple signaling pathways triggered by IL-4 signaling, as previously

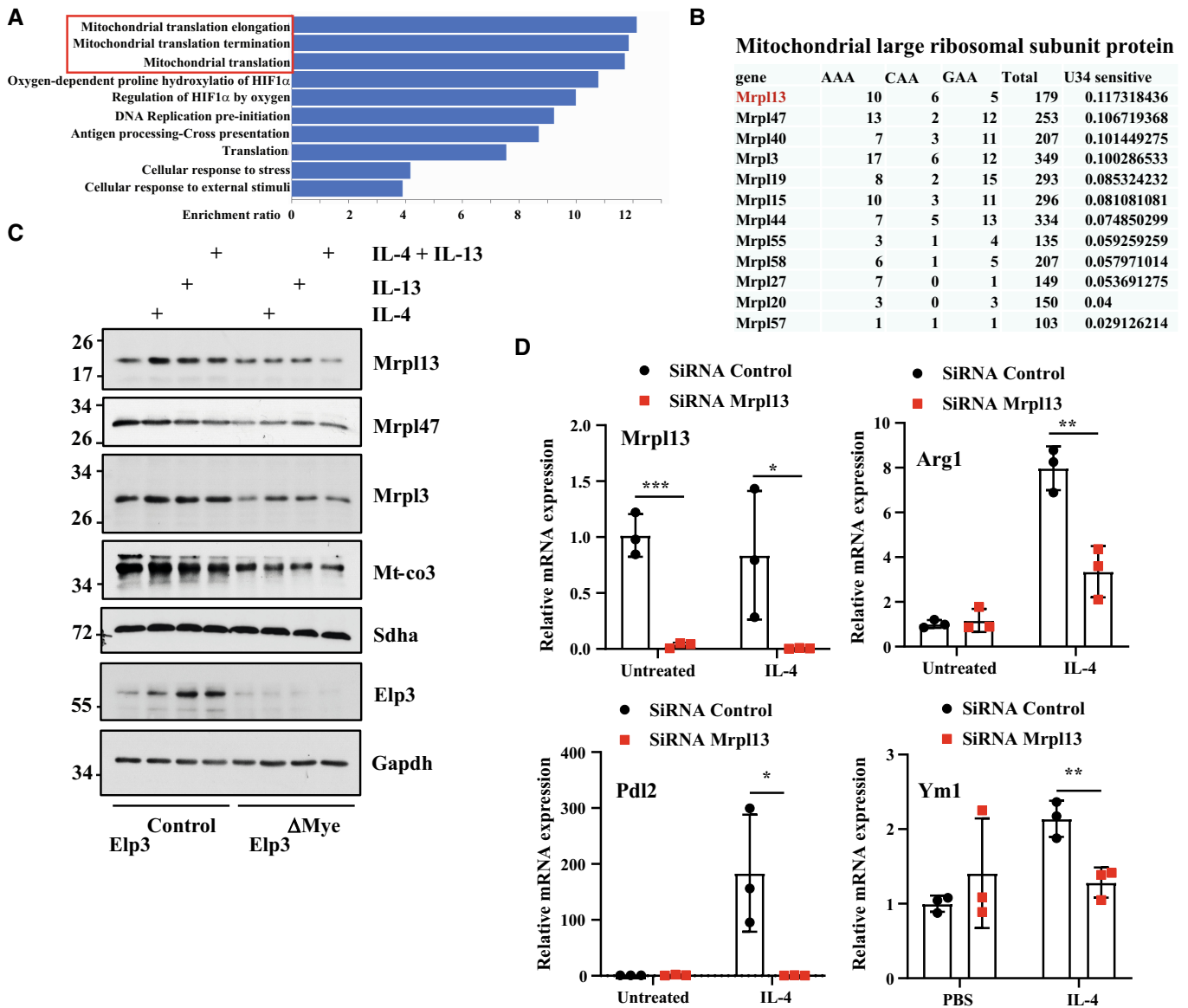


Figure 8. Elp3 controls the expression of some mitochondrial proteins.

A Enrichment of candidates involved in mitochondrial translation in the proteomic signature of 206 candidates (Reactome pathway enrichment analysis).
 B Enrichment of Mrpl proteins in the proteomic signature of 206 candidates. Proteins were classified according to the combined frequency of AAA, GAA, and CAA codons in their open reading frame.
 C Elp3 promotes mitochondrial translation. BMDMs from the indicated genotypes were treated or not with IL-4/IL-13 (10 ng/ml) for the indicated hours and the resulting cell extracts were subjected to WB analyses.
 D Impaired expression of M2 markers upon Mrpl13 deficiency in IL-4-stimulated macrophages. BMDMs were transfected with a control siRNA or with a siRNA targeting Mrpl13 and the resulting cells were untreated or stimulated with IL-4 (10 ng/ml) for 24 h. mRNA levels of the indicated candidates were quantified by Real-Time PCR experiments. mRNA levels in unstimulated BMDMs transfected with the control siRNA were set to 1 and levels in other experimental conditions were related to that. Experiments were conducted in triplicates (mean \pm SD, Student t-test, *** P < 0.001, ** P < 0.01, * P < 0.05).

Source data are available online for this figure.

reported for Irf4 (Huang *et al*, 2016). Interfering with Elp3 or Ctub2 expression has dramatic consequences on cascades induced by polarizing signals and consequently on downstream expression of M1 or M2 markers. Likewise, metabolic reprogramming linked to macrophage polarization is also dramatically deregulated upon Elp3

deficiency. Although Ctub2 expression is not changed upon stimulation by M1 polarizing signals, Ctub2 deficiency impairs Ctub1 function and consequently the thiolation of some U₃₄ tRNAs. As a result, Ctub2 and Elp3 deficiencies share common consequences on macrophage polarization.

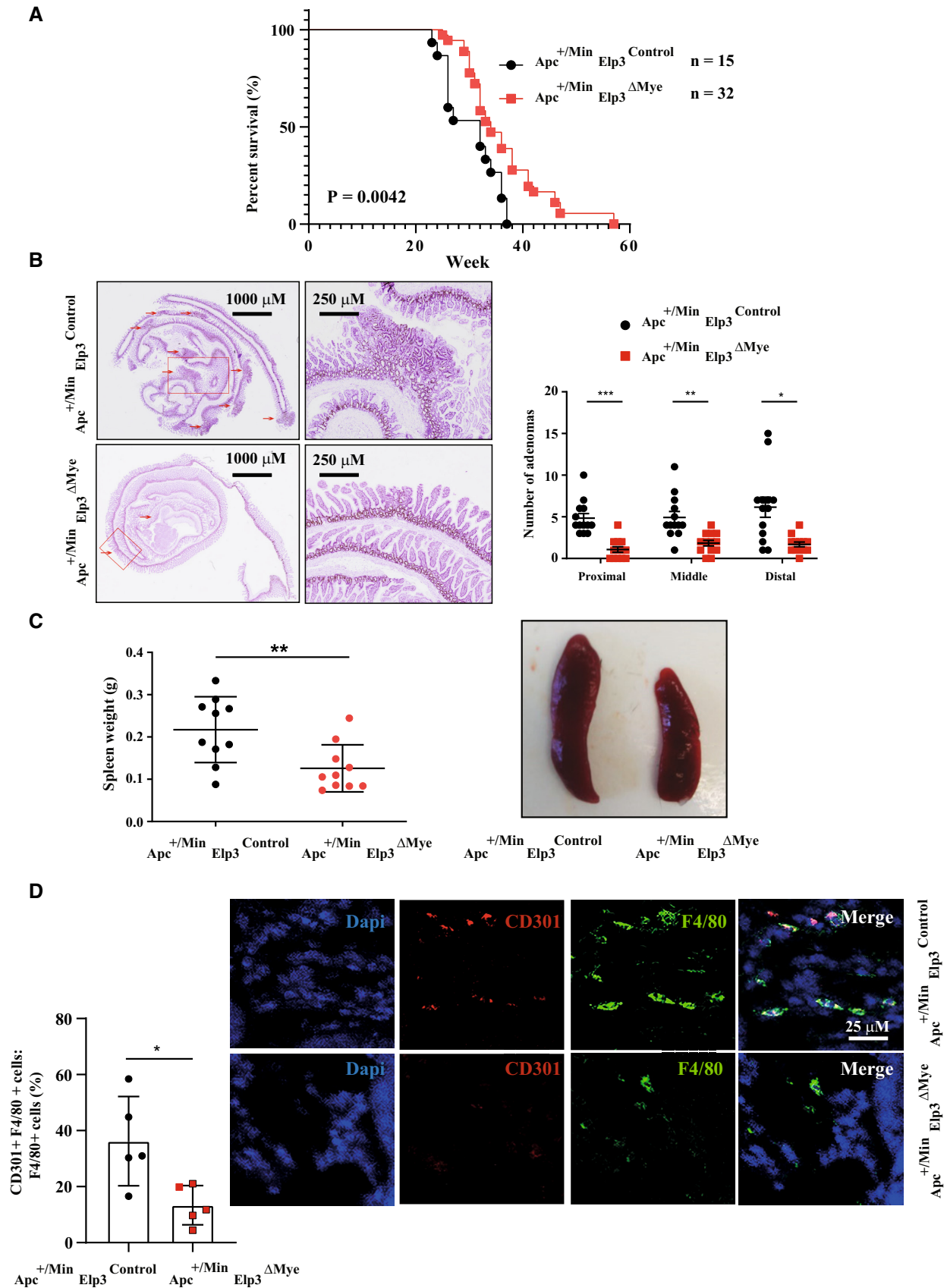


Figure 9.

Figure 9. Elp3 expression in myeloid cells promotes Wnt-driven tumor initiation in the intestine.

- A, B *Elp3* deficiency in myeloid cells prolongs survival of *Apc*^{+/-Min} mice (A) and reduces the number of adenomas in all parts of the intestine (B). A Kaplan–Meyer curve was established with the indicated genotypes (A). The number of intestinal tumors in the indicated parts of the intestine was quantified in both *Apc*^{+/-Min} *Elp3*^{Control} and *Apc*^{+/-Min} *Elp3*^{ΔMye} mice (B) (*n* = 10 mice per genotype; mean ± SD, Student *t*-test, ****P* < 0.001, ***P* < 0.01, **P* < 0.05). Representative H&E analyses of intestinal crypts from the indicated genotypes are illustrated.
- C *Elp3* deficiency in myeloid cells decreases the spleen weight of *Apc*^{+/-Min} mice (*n* = 10 mice per genotype; mean ± SD, Student *t*-test, ***P* < 0.01). Representative pictures of the spleen from the indicated genotypes.
- D *Elp3* expression in myeloid cells maintains the pool of tumor-associated macrophages (TAMs). The number of TAMs, defined as CD301⁺/F4/80⁺ cells among F4/80⁺ cells was quantified in intestinal crypts from both *Apc*^{+/-Min} *Elp3*^{Control} and *Apc*^{+/-Min} *Elp3*^{ΔMye} mice (*n* = 5 mice per genotype; mean ± SD, Student *t*-test, **P* < 0.05). Representative immunofluorescence analyses are illustrated.

Source data are available online for this figure.

The phenotype that results from *Elp3* deficiency in macrophages undergoing M1 or M2 polarization resembles what has been reported without mTORC2 activation. Indeed, Akt phosphorylation on serine 473, a residue targeted by mTORC2 upon LPS/IFN γ stimulation, is impaired without *Elp3*. Moreover, both *Elp3* and *Rictor* deficiencies show elevated levels of cytokines linked to M1 macrophage polarization (Festuccia *et al*, 2014). Likewise, the phosphorylation of Akt by mTORC2, the transcriptional signature and metabolic reprogramming by IL-4 are impaired without *Elp3*, as previously reported without mTORC2 (Huang *et al*, 2016). Collectively, these data define a biological context in which *Elp3* promotes mTORC2 signaling, as demonstrated in yeast (Candiracci *et al*, 2019). As *Ctu2*, a tRNA-modifying enzyme acting in the same cascade as *Elp3*, also promotes mTORC2 activation, it is likely that these enzymes are required for the translation of mRNA candidates acting as activators of mTORC2. In this context, we identified *Ric8b*, a candidate known to promote mTORC2 activation (Nagai *et al*, 2020), as a direct target of *Elp3*. *Ric8b* expression is induced by IL-4 in macrophages, similarly to *Elp3*. Moreover, *Elp3* deficiency interferes with *Ric8b* expression in IL-4-stimulated macrophages. *Ric8b* is enriched in codons (9.45%) known to rely on *Elp3* to be properly translated. Our data based on experiments conducted with a *Ric8b* mutant lacking all Lys^{AAA}, Gln^{CAA}, and Glu^{GAA} codons demonstrate that *Elp3* promotes *Ric8b* translation in a codon-dependent manner. Alternatively, *Elp3* may have stabilized *Ric8b* through mTORC2. Such hypothesis indeed explains how *Elp3* stabilizes the anti-apoptotic protein *Mcl-1* in triple negative breast cancers (Cruz-Gordillo *et al*, 2020). The PI3K/mTOR pathway indeed stabilizes candidates such as *Mcl-1* (Wang *et al*, 1999). Therefore, *Elp3* may also regulate protein stability of a variety of candidates downstream of mTORC2, in addition to promoting mRNA translation in a codon-dependent manner.

Elp3 may also promote mTORC2 activation through additional, *Ric8b*-independent pathways. Indeed, a careful analysis of candidates whose protein but not mRNA levels are impaired in IL-4-stimulated BMDMs lacking *Elp3* revealed *Rps6* whose deficiency attenuates insulin-induced mTORC2 activation (Yano *et al*, 2014).

Beside a role of *Elp3* in mTORC2 activation, *Elp3* also regulates early steps of IL-4 signaling. Indeed, both *Tyk2* and *Stat6* phosphorylation triggered by IL-4, which occur through a mTORC2-independent pathway, are defective upon *Elp3* deficiency. One explanation could be the decreased IL-13R α 1 expression in *Elp3*-depleted peritoneal macrophages. Alternatively, elevated *Socs1* levels seen without *Elp3* could also underlie defective *Stat6* phosphorylation, a mechanism also reported upon *Rictor* deficiency

(Hallowell *et al*, 2017). It remains to be demonstrated how *Elp3* regulates both *Socs1* and IL-13R α 1 expression though.

Elp3 deficiency leads to protein misfolding and aggregation in both yeast and human (Nedialkova & Leidel, 2015; Rapino *et al*, 2018). Interestingly, candidates found in these aggregates are enriched in codons decoded by tRNAs lacking mcm⁵s²U₃₄ modifications in *Elp3*-deficient yeast (Tavares *et al*, 2020). Therefore, it is tempting to speculate that defects in macrophage polarization seen upon *Elp3* deficiency may result, at least in part, from misfolding of a variety of proteins acting downstream of both LPS/IFN γ and IL-4 signaling cascades. In support with this hypothesis, we found that several mitochondrial proteins of ribosome large subunit such as *Mrpl3*, *Mrpl13*, and *Mrpl47* accumulate in aggregates of macrophages stimulated with IL-4 upon *Elp3* deficiency. As a result, mitochondrial translation is impaired, as evidenced by decreased protein levels of candidates such as *Mt-co3*. This finding has important consequences as the depletion of *Mrpl13* also leads to defects in M2 macrophage polarization, similarly to *Elp3* deficiency. Therefore, our results demonstrate how critical mitochondrial translation regulated by a tRNA-modifying enzyme is in macrophage polarization.

The loss of *Elp3* in cortical progenitors, T cells as well as in the hematopoietic system causes *Atf4* stabilization, which largely underlies the phenotypical defects in mice (Laguesse *et al*, 2015; Lemaitre *et al*, 2021; Rosu *et al*, 2021). We have not seen any robust *Atf4* stabilization in peritoneal macrophages lacking *Elp3* expression, suggesting that *Atf4* stabilization is not a systematic consequence of *Elp3* deficiency in primary cells.

The capacity of *Elp3* to prevent aberrant M1 macrophage polarization defines U₃₄ chemical tRNA modifications as an anti-inflammatory process as *Elp3* deficiency in myeloid cells exacerbates inflammation in a model of experimental colitis. The defective Akt-dependent FoxO1 phosphorylation seen in LPS/IFN γ -stimulated peritoneal macrophages most likely contributes to this inflammatory phenotype seen upon *Elp3* deficiency. Therefore, *Elp3* expression in myeloid cells prevents excessive inflammation in the large intestine, at least by promoting mTORC2 activation.

Loss of *Elp3* in macrophages impacts on mitochondrial functions. Indeed, IL-4-dependent metabolic reprogramming, a feature of M2 macrophage polarization, is largely impaired without *Elp3*. TCA cycle and mitochondrial oxidative phosphorylation are defective upon *Elp3* deficiency in macrophages. These phenotypes can be explained, at least in part, by a defective activation of both IL-4R α -*Stat6*- and mTORC2-Irf4-dependent pathways, given their key roles in glucose consumption occurring during IL-4-dependent

metabolic reprogramming (Huang *et al*, 2016). The fact that Elp3 promotes the production of some mitochondrial proteins of ribosome large subunit induced by IL-4 represents one molecular mechanism by which Elp3 controls mitochondrial functions in metabolic reprogramming.

Lastly, the genetic inactivation of *Elp3* in myeloid cells delays Wnt-driven tumor initiation in the intestine. This delay in tumor development also occurs when *Elp3* is inactivated in intestinal epithelial cells (Ladang *et al*, 2015). Although the role of Elp3 in all stromal cells remains to be extensively defined, our data strengthen the notion that Elp3 is a promising therapeutic target to treat intestinal tumors showing constitutive Wnt signaling.

Materials and Methods

Cell lines and reagents

RAW 264.7 cells were from ATCC (ATCC TIB-71) and were tested several times for mycoplasma contamination. They were cultured in DMEM medium supplemented with 10% FBS, 4.5 g/l of glucose, 2 mM of Glutamine, and 100 U/ml of Penicillin/Streptomycin. LPS was purchased from Sigma (L4391) and mouse IFN γ , IL-4, and IL-13 were from R&D Systems (485-MI, 404-ML, and 413-ML). Wortmannin (W1628) and AS1517499 (SML1906) were purchased from Sigma. Flag-Ric8b WT and Flag-Ric8b MUT were generated by VectorBuilder using the pLV-Puro-CMV/T7-EGFP as a lentiviral vector backbone.

Mice

The *Elp3*^{lox/lox} mouse was previously described (Ladang *et al*, 2015). The LysM-CRE strain was obtained from Jackson Laboratory (stock 004781). *Elp3*^{ΔMye} mice were obtained by crossing *Elp3*^{lox/lox} with the LysM-CRE strain while *Elp3*^{Control} mice correspond to *Elp3*^{lox/lox} mice. The *Elp3*^{ΔIEC} mice in which Elp3 expression is genetically inactivated in intestinal epithelial cells has been previously described (Ladang *et al*, 2015). All mouse strains were housed at the animal facility of the University of Liege, according to rules requested by the ethical comity (file number 2332). Cages were ventilated, softly lit, and subjected to a light dark cycle. The relative humidity was kept at 45–65%. Mouse rooms and cages were always kept at a temperature range of 20–24°C. *Apc*^{+/-Min} mice were obtained from Jackson Laboratory (strain #:002020).

Experimental colitis model

Mice were given 2.5% DSS (molecular mass 36,000–50,000, MP Biomedicals, LLC) in the drinking water for 6 continuous days. Body weight was observed daily. Six days after the administration of DSS in water, colon length was measured and the colonic histological score was evaluated as follows: Inflammatory cell infiltrate severity (0–3) and extent (0–3), hyperplasia (0–2) and epithelial erosion (0–3), according to hematoxylin and eosin (H&E) staining samples, as previously described (Erben *et al*, 2014). mRNAs were extracted from the distal 1 cm of colon. For survival record, mice were given 2.5% DSS for 7 continuous days, then followed with normal water for another 8 days.

Generation of BMDMs

Bone marrow was extracted from femur and tibia, after lysis of erythrocytes, marrow cells were cultured in complete medium consisting of Dulbecco's modified Eagle's medium with 30% L929-conditioned medium and 10% heat-inactivated fetal bovine serum. On day 4, nonadherent cells were removed and the medium was replaced. On day 7, BMDMs were treated with stimulators. For infections of BMDMs, 3×10^6 293-LentiX cells were transfected with 12 μ g of the "GFP" lentiviral plasmid (used as negative control), with Ric8b WT or Ric8b MUT, 12 μ g of psPAX2 and 5 μ g of VSVG plasmid, using the Mirus Bio's TransIT-LT1 reagent. Supernatants of those infected cells were collected and filtered (0.2 μ m) 72 h after transfection and centrifuged at 90,000 g for 4 h. Pellets were diluted in BMDM growth media for 4 h at 4°C with constant rocking. Virus was added to BMDMs on the 6th day of differentiation with 8 μ g/ml of polybrene. Twenty-four hours later, the media was changed and cells were left for another 96 h. After that, cells were collected and subjected to western blot analyses.

Treatment of mice with thioglycollate and peritoneal macrophage isolation

A 3% solution of thioglycollate (BD, Cat: 211716) was prepared in water, autoclaved and mice were received 1 ml intraperitoneal injection (i.p.) to induce peritonitis 4 days before sacrifice. Following sacrifice, peritoneal cavity exudate cells were obtained by washing the cavity with cold 1X PBS, erythrocytes were removed by incubating with a red blood cell lysis buffer. Cells were seeded in 6 well plates in the same culture medium as RAW 264.7 cells. Two hours later, cells were washed by PBS and then used for subsequent experiments.

IL-4 complex administration

Recombinant mouse IL-4 (BioLegend) was mixed with anti-mouse IL-4 monoclonal antibody (Biolegend, 11B11) at a molar ratio of 1:5 and incubated at room temperature (RT) for 5 min. Mice were injected i.p. with 100 μ l of this cytokine-antibody complex (IL-4c) containing 5 μ g of rIL-4 and 25 μ g of anti-IL-4 antibody or PBS as control on day 0 and day 2. Peritoneal exudate cells were collected on day 4.

FACS sorting and intracellular staining

Peritoneal lavage was performed to collect exudates. Cells were then stained with primary antibodies in the Table EV1 before dead cells were excluded using a fixable viability dye (2000x, eFluor™ 780, eBiosciences Cat # 65-0865-14). A total of one million peritoneal macrophages were then sorted as Live F4/80⁺CD11b⁺ cells using a FACSAria VIII (BD Biosciences) for further RNA extraction.

For Ki67 staining, the eBioscience FoxP3/Transcription Factor Staining Buffer set (00-5523-00) was used. In brief, after surface staining, cells were fixed with 1 \times Fix Concentrate buffer in the provided Fix Diluent for 30 min at room temperature. To permeabilize the cells, samples were washed with 1 \times Perm buffer diluted in water. Then, the samples were stained with secondary antibodies 20 min at room temperature, followed by washing in 1 \times Perm buffer and FACS buffer before flow cytometry.

For EdU staining, mice were given 1 mg of EdU i.p. (from Click-iT™ Plus EdU Flow Cytometry Assay Kit, Thermo Fisher, C10635) 3 h before sacrifice. After sacrifice of mice and peritoneal lavage, samples were processed, fixed. EdU-labeled cells were washed in 1× Perm buffer, incubated in Edu detection reaction cocktails for 30 min at room temperature, followed by washing in 1× Perm buffer and FACS buffer.

Histology and immunofluorescence microscopy

For histopathological analysis, colon samples were embedded in paraffin wax then sectioned (5 μm) and stained with H&E. For immunofluorescence, after dewaxing and hydration, antigen retrieval was performed by boiling slices for 30 min in a sodium citrate buffer pH 6.0. Slides were blocked with 10% goat serum for 1 h at RT and incubated with primary antibodies at 4°C overnight. After washing, Alexa Fluor® 568 goat anti-rabbit and Alexa Fluor® 488 goat anti-rat (Thermo Fisher) secondary antibody was applied to the slides at RT for 1 h. Then, sections were counterstained with 4', 6-diamidino-2-phenylindole (DAPI). The antibody used in this study are listed in Table EV1. The immunofluorescence staining data were analyzed by using the Image-pro plus software.

RNA extraction and Real-Time PCR analysis

mRNAs expression was defined by reverse transcription polymerase chain reaction and RT-qPCR. RNAs were isolated from tissue or cells with the RNeasy Mini Kit (Qiagen) and then synthesized to DNAs (cDNAs) by using the RevertAid H Minus First Strand cDNA Synthesis Kit (Thermo Fisher) and augmented by using SYBR Green qPCR Mix (TAKARA) on LightCycler 480 (Roche). ΔCt values were normalized to GAPDH, and relative quantification of gene expression were compared to WT group. The primers used in this study are listed in Table EV2 and synthesized by Integrated DNA Technologies (Germany).

Immunoblotting

Macrophages were washed 3 times in cold PBS, lysed in RIPA buffer with protease and phosphatase inhibitor cocktails (Roche) for 10 min on a rocker 100 rpm at 4°C. Protein concentrations were quantified by using a BCA protein kit (Thermo Fisher). Proteins samples were analyzed on SDS polyacrylamide gel electrophoresis (SDS-PAGE) and transferred onto PVDF membranes (Millipore). These membranes were blocked with 5% BSA (Cell signaling) and 0.1% Tween 20 in Tris-buffered saline 1 h, and then incubated overnight at 4°C with primary antibodies. The appropriate HRP-coupled secondary antibody was then added and was detected with chemiluminescent substrate ECL (Thermo Fisher).

Quantification of tRNA modifications

BMDMs were collected and cultured from three *Elp3*^{Control} and *Elp3*^{AMye} mice. Replicates were used for each mouse. Total RNAs were extracted using Trizol. RNAs were submitted to Arraystar (arraystar.com) for LC-MS analysis where it was processed as follows: total RNA samples were quantified by using Nanodrop ND-1000. tRNAs were isolated from total RNAs by Urea-PAGE and 60-

90 nt bands of tRNAs were excised and purified by ethanol precipitation. tRNAs were hydrolyzed to single dephosphorylated nucleosides by enzyme mix. Pretreated nucleoside solutions were deproteinized using Satorius 10,000-Da MWCO spin filter. The analysis of nucleoside mixtures was performed on Agilent 6460 QQQ mass spectrometer with an Agilent 1260 HPLC system using the Multi reaction monitoring (MRM) detection mode. LC-MS data were acquired using Agilent Qualitative Analysis software. MRM peaks of each modified nucleoside were extracted and normalized.

Northern blots

Five micrograms of total RNAs (or 1 μg of enriched small RNAs isolated using the kit mirVana™ Paris™ RNA (Invitrogen)) extracted from peritoneal macrophages were subjected to electrophoresis on a 8% acrylamide gel (29:1) with 6 M Urea and 1 × TBE. Fifty micrograms per milliliter of N-acryloylaminophenyl mercuric chloride (APM) were added or not. RNAs were transferred on a positively charged nylon membrane (180 mA, 45 min, 0.5 × TBE) using the Trans Blot Turbo Transfer system. RNAs were crosslinked using a Spectrolinker UV crosslinker (Invitrogen). Hybridization was performed using the Easy-Hyb solution (Roche). The probe dQ(UUG) GGTCCACCGAGATTT-GAACTCGG, tK(UUU)CCTGAACAGGGACT TGAACCCTGA-3 or tE(UUC) GTTCCACACCGGGAGTC-GAAC was labeled using the DIG Oligonucleotide 3' end labeling kit (second generation) and hybridized overnight at 50°C with constant rotation (for the probe tK(UUU), the hybridization was performed at 45°C). Membranes were washed twice with a buffer containing 2 × SSC, 0.1% SDS at room temperature during 5 min and twice with another buffer containing 0.2 × SSC, 0.1% SDS at 50°C (45°C for the probe tK(UUU)) during 15 min. The detection of both unmodified and thiolated tRNAs was performed using DIG Luminescent Detection Kit for Nucleic Acids.

ChIP

ChIP assays were essentially performed by using the anti-STAT6 antibody (Cell signaling) or an IgG antibody as negative control. Extracts from PBS or IL-4-treated RAW 264.7 cells were precleared by incubation with protein A Sepharose/Herring sperm DNA for 1 h and subsequent IPs were performed by incubating cell extracts overnight at 4°C with the relevant antibody followed by 1 h of incubation with protein A/Herring sperm DNA. Protein-DNA complexes were washed as per standard ChIP techniques. After elution, proteinase K treatment and reversal of crosslinks, DNA fragments were analyzed by real-time PCR with SYBR green detection. Input DNA was analyzed simultaneously and used for normalization purposes. Primers used to address STAT6 recruitment on the *Elp3* gene promoter are listed in the Table EV2. Putative STAT6-binding sites were predicted by JASPAR database (<http://jaspar.genereg.net/>).

Transfection of siRNA

Cells were transfected with ON-TARGETplus Mouse Raptor, Rictor, Ric8b, and siGENOME mouse *Elp3* and *Ctu2* siRNAs (Horizon Discovery) or control siRNAs by using INTERFERIN (Polplus) according to the manufacturer's instruction. RAW264.7 cells and BMDMs were transfected with 50 nmol siRNA and 10 μl of transfection reagent on

three consecutive days and experiments were performed 96 h after the first transfection. The siRNAs and their sequences used in this study are listed in Table EV3.

RNA sequencing and analysis

BMDMs from *Elp3*^{Control} and *Elp3*^{AMye} mice were treated with or without IL-4 and IL-13 for 2 h. A total of 6 mice were used for each experimental condition. Total RNAs were extracted using a RNeasy Mini Kit (Qiagen) according to the manufacturer's instructions. RNA quality was controlled on the Bioanalyser 2100 (Agilent). TruSeq mRNA library preparation started from 1 µg of total RNA and denatured for 4 min. Libraries were validated by qPCR using the KAPA Universal kit (KAPA Biosystems). Libraries were sequenced on the NextSeq550. We employed GSEA in the context of gene ontology and utilized specific genes sets (GEO: GSE7348 and GSE25123) to perform GSEA. The heatmap was generated using <https://software.broadinstitute.org/morpheus>. Differential gene expression was calculated using DESeq2 in R. Genes with normalized *P* values < 0.05 were considered as significantly regulated.

LC-MS profiling for intracellular metabolites

For metabolomics analysis of peritoneal macrophages, the peritoneal macrophages from *Elp3*^{Control} and *Elp3*^{AMye} mice were treated with or without IL-4 and IL-13 for 24 h. Each sample was washed three times with cold PBS, collected into an Eppendorf tube, frozen in liquid nitrogen and stored at -80°C until extraction. The extraction solution used was 50% methanol, 30% ACN, and 20% water. The volume of extraction solution added was calculated from the cell count (2×10^6 cells/ml). After addition of extraction solution, samples were vortexed for 5 min at 4°C, and immediately centrifuged at 16,000 g for 15 min at 4°C. The supernatants were collected and analyzed by liquid chromatography-mass spectrometry using SeQuant ZIC-pHilic column (Merck) for the liquid chromatography separation. Mobile phase A consisted of 20 mM of ammonium carbonate plus 0.1% ammonia hydroxide in water. Mobile phase B consisted of ACN. The flow rate was kept at 100 ml/min, and the gradient was 0 min, 80% of B; 30 min, 20% of B; 31 min, 80% of B; and 45 min, 80% of B. The mass spectrometer (QExactive Orbitrap, Thermo Fisher Scientific) was operated in a polarity switching mode and metabolites were identified using TraceFinder Software (Thermo Fisher Scientific). To obtain a robust statistical analysis, metabolomics data were normalized using the median normalization method (Hendriks *et al*, 2007). The data were further pre-processed with a log transformation. The MetaboAnalyst 4.0 software (Xia *et al*, 2015) was used to conduct statistical analysis and heatmap generation, and enrichment analysis. The algorithm for heatmap clustering was based on the Pearson distance measure for similarity and the Ward linkage method for biotype clustering. Metabolites with similar abundance patterns were positioned closer together.

Glucose consumption assay

Glucose-Glo™ Assay Kit (Promega) was used to determine glucose uptake according to the manufacturer's protocols. IL-4-primed M2 peritoneal macrophages from *Elp3*^{Control} and *Elp3*^{AMye} mice were plated at 2.5×10^5 cells/ml into 24-well plates and incubated for

24 h. Next day, cells incubation mediums and medium without cells (empty control) were collected and used for determination of glucose consumption. The luminescence was recorded by PerkinElmer Victor X3. The glucose consumption was calculated as the difference between the noncells medium value and cells incubation medium value.

Complex I enzyme activity assay

The Complex I enzyme activity was performed by following instructions of the Complex I Enzyme Activity Microplate Assay Kit (Abcam, ab109721). Briefly, 1×10^7 peritoneal macrophages from *Elp3*^{Control} and *Elp3*^{AMye} mice were seeded in 15 cm² dishes with IL-4 treatment for 24 h. The cell lysis buffer was added into the microplate and incubated at room temperature for 3 h. After 3 washes, assay solutions were added and then the data were recorded as the following settings: wavelength, 450 nm; time, 30 min; interval, 20 s. The rate was calculated by the formula: $\text{mOD}/\text{min} = \text{Abs } 1 - \text{Abs } 2 (\text{mOD @ } 450 \text{ nm}) / \text{Time } 1 - \text{Time } 2 (\text{minutes})$.

Mitochondrial membrane potential

Peritoneal macrophages from *Elp3*^{Control} and *Elp3*^{AMye} mice were plated at 5×10^5 cells/ml in 12-well plates and treated with IL-4 for 24 h. The following control cell samples were accounted for: unstained, single stained TMRM (Thermo Fisher), MitoTracker Deep Red (Thermo Fisher, hereafter MTDR), and Viability 405/452 Fixable Dye (Miltenyi Biotech). Cells were stained with Viability 405/452 Fixable Dye at 37°C in the dark for 30 min. Next, cells were stained by a mix of MTDR (50 nM) and TMRM (20 nM) at 37°C in the dark for another 30 min. Cells were removed from the plate surface using a cell scraper and transferred to polypropylene FACS tubes. Cells were then analyzed using BD FACS Canto II, and data were analyzed using FlowJo software.

Extracellular flux assays

All experiments were performed with a Seahorse XFp extracellular flux analyzer (Agilent). Cells were seeded (100,000 cells/well) in XFp mini-plates (Agilent) and treated by IL-4 for 24 h. One hour before the mitochondrial oxygen consumption rate (OCR - pmol/min) analysis, culture medium was replaced by an unbuffered serum-free DMEM (Basal DMEM, Agilent) supplemented with pyruvate (1 mM), glutamine (2 mM), glucose (10 mM), pH7.4, and further incubated at 37°C in ambient CO₂ incubator. During the assay, cells were successively stressed with oligomycin (1 µM), FCCP (1.0 µM) and rotenone/antimycin A (0.5 µM each) mix. Spare OCR capacity was calculated as the difference between the average of the 3 pre-oligomycin measurements and the average of the 3 post-FCCP measurements. All results were normalized according the cell number evaluated by Hoechst (2 µg/ml) incorporation (A.U.) after cold methanol/acetone fixation. Results shown are representative of 3 independent experiments.

Puromycin proximity ligation assay (Puro-PLA)

IL-4-activated BMDMs were treated with Puromycin (10 µg/ml) for 5 min at 37°C, 5% CO₂, and washed twice in PBS. As negative

control, cells were treated with Cycloheximide (100 µg/ml) before Puromycin treatment. Cells were fixed in 4% paraformaldehyde for 20 min and permeabilized with 0.5% Triton X-100 solution for 1 h. Duolink PLA reagents (Sigma-Aldrich) were used to detect newly synthesized proteins according to the manufacturer's instructions. Briefly, cells were blocked using the Duolink Blocking solution for 1 h at room temperature and then were incubated in the primary antibody (anti-Ric8b) overnight at 4°C. After several washings, cells were incubated in the PLUS and MINUS PLA probes solutions for 1 h at 37°C. Next, cells were incubated in the ligation solution (30 min) and in the amplification buffer (100 min) at 37°C. Once the amplification was done, cells were incubated in the anti- α -tubulin antibody solution overnight and then incubated in the secondary antibody solution for 1 h. Glasses were mounted with the fluorescent mounting medium overnight. Duolink PLA signals were visualized by fluorescence microscopy (Zeiss HR LSM 880).

Aggresome detection

BMDMs were treated with IL-4 for 24 h and the positive control was treated by MG-132. Then, the procedures were followed in agreement with the instruction of the PROTEOSTAT® Aggresome Detection Kit (Enzo, ENZ-51035-K100). Briefly, cells were washed by PBS twice and then incubated in 4% formaldehyde for 30 min. Cells were then washed with PBS and incubated in the Permeabilizing Solution for 30 min and lastly incubated in the Dual Detection Reagent for another 30 min in the dark. The samples were analyzed in the FL3 channel of a flow cytometer.

Aggregates isolation

BMDMs were treated with IL-4 or PBS for 24 h and cells were lysed using the Cytoplasmic Lysis Buffer (Tris HCl pH 7.9, 10 mM; sucrose 340 nM; CaCl₂ 3 mM; EDTA 0.1 mM; MgCl₂ 2 mM; 1 mM DTT; 0.5% NP-40) for 10 min on ice. The samples were then centrifuged at 1,100 g, 4°C for 15 min. The supernatant was centrifuged at 20,000 g, 4°C for 10 min. Protein concentration in supernatants was determined with the Bio-Rad Protein Assay. Protein concentration was equalized across samples and aggregates were pelleted from equal amounts of total proteins. Pellets were sonicated 4 times for 8 min in the cold room. The samples were then centrifuged at 16,000 g, at 4°C for 20 min and the pellets were washed using the washing buffer (NaF 20 mM pH 6.8; PMSF 1 µM) with 2% NP-40 twice and next washed using the washing buffer without NP-40 one more time. Lastly, the samples were sonicated for 4 min and centrifuged at 16,000 g, at 4°C for 20 min. Supernatants were collected as aggregates fraction.

LC-MS profiling for total proteins and aggregates proteins

The total proteins were extracted from *Elp3*^{Control} and *Elp3*^{AMye} BMDMs treated with or without IL-4 (20 ng/ml) for 4 h. Lysates were quantified by Qubit fluorometry. The aggregate extraction samples were heated at 100°C for 15 min in the loading buffer, centrifuged briefly, and 50% was loaded on gel. Each gel lane was excised into 20 equally sized segments and gel slices were processed using a robot (ProGest, DigiLab) with the following protocol: washed with 25 mM ammonium bicarbonate followed by

acetonitrile; reduced with 10 mM dithiothreitol at 60°C followed by alkylation with 50 mM iodoacetamide at room temperature; digested with trypsin (Promega) at 37°C for 4 h; quenched with formic acid and the supernatant was analyzed directly without further processing. Peptides were analyzed by nano LC/MS/MS with a Waters NanoAcquity HPLC system interfaced to a Thermo Fisher Fusion Lumos. Peptides were loaded on a trapping column and eluted over a 75 µm analytical column at 350 nL/min; both columns were packed with Luna C18 resin (Phenomenex). The mass spectrometer was operated in data-dependent mode, with MS and MS/MS performed in the Orbitrap at 60,000 FWHM resolution and 15,000 FWHM resolution, respectively. APD was turned on. The instrument was run with a 3 s cycle for MS and MS/MS. Mascot DAT files were parsed into the Scaffold software for validation, filtering and to create a nonredundant list per sample. Data were filtered 1% protein and peptide level FDR and requiring at least two unique peptides per protein.

Codon bias analysis

The coding sequence (cds) of all protein-coding *Mus musculus* genes (genome assembly GRCm38.p6) was downloaded from Ensembl (<http://www.ensembl.org>). Codon frequency of AAA, CAA, and GAA in the complete cds of every Mouse Genome Informatics-annotated mouse gene was computed using the seqinr and biomaRt packages in R. We next computed a z-score for AAA, CAA, and GAA codon enrichment/ depletion in the cds of proteins found to be downregulated in BMDMs from *Elp3*^{AMye} mice in our comparative proteomic analysis using the formula: $z = (\text{codon frequency of gene} - \text{average codon frequency in all mouse cds}) / \text{variance of codon frequency in all mouse cds}$. A heatmap was subsequently generated using the heatmap package in R.

Statistical analysis

The statistical significance of differences in groups were performed using the GraphPad Prism 8.0 Software. All data and error bars are presented as the mean \pm standard deviation (SD) and based on experiments performed at least in triplicate. The one- or two-way ANOVA test was used to compare the mean of a continuous variable between two samples and Unpaired Student's *t*-test was used to comparison between two groups. $P < 0.05$ was considered to be statistically significant. Blinding was systematically done.

Data availability

RNA-seq data has been deposited on Gene Expression Omnibus (GEO) under accession number GSE166169 (<http://www.ncbi.nlm.nih.gov/geo/query/acc.cgi?acc=GSE166169>). Proteomic data has been deposited on ProteomeXChange with accession code PXD033962 and PXD023588 (<http://www.ebi.ac.uk/pride/archive/projects/PXD033962>; <http://www.ebi.ac.uk/pride/archive/projects/PXD023588>). Other data that support the findings of this study are available from the corresponding authors upon request.

Expanded View for this article is available [online](#).

Acknowledgments

The authors are grateful to the GIGA Imaging platform for the FACS analyses. They also thank Dr. Zhang from NIBIO (Oslo, Norway) for providing us R scripts on RNA-seq and proteomics analysis. This work was supported by grants from WELBIO (WELBIO-CR-2019C-02R), FNRS/TELEVIE, the Belgian Foundation against Cancer (FBC/2020/1323), the University of Liege (ARC UBICOREAR) and by the Leon Fredericq Foundation (Faculty of Medicine, CHU of Liege). PC and AC are Senior Research Associate and Research Director at the FNRS, respectively.

Author contributions

Dawei Chen: Conceptualization; formal analysis; validation; investigation.
Ivan Nemazanyy: Investigation; methodology. **Olivier Peulen:** Investigation; methodology. **Kateryna Shostak:** Data curation; formal analysis; supervision; validation; investigation; methodology. **Xinyi Xu:** Formal analysis; methodology. **Seng Chuan Tang:** Formal analysis; methodology. **Caroline Wathieu:** Data curation; methodology. **Silvia Turchetto:** Formal analysis; methodology. **Sylvia Tielens:** Data curation; methodology. **Laurent Nguyen:** Conceptualization; formal analysis; methodology. **Pierre Close:** Methodology. **Christophe Desmet:** Conceptualization; resources. **Sebastian Klein:** Conceptualization; data curation; formal analysis; methodology. **Alexandra Florin:** Data curation; methodology. **Reinhard Büttner:** Conceptualization; data curation; methodology. **Georgios Petrellis:** Data curation; formal analysis. **Benjamin Dewals:** Conceptualization; data curation; formal analysis; supervision; validation; investigation; methodology; writing – review and editing. **Alain Chariot:** Conceptualization; resources; data curation; formal analysis; supervision; funding acquisition; validation; investigation; visualization; methodology; writing – original draft; project administration; writing – review and editing.

Disclosure and competing interests statement

The authors declare that there is no conflict of interest.

References

- Bauer F, Matsuyama A, Candiracci J, Dieu M, Scheliga J, Wolf DA, Yoshida M, Hermand D (2012) Translational control of cell division by elongator. *Cell Rep* 1: 424–433
- Brown J, Wang H, Suttles J, Graves DT, Martin M (2011) Mammalian target of rapamycin complex 2 (mTORC2) negatively regulates toll-like receptor 4-mediated inflammatory response via FoxO1. *J Biol Chem* 286: 44295–44305
- Brunet A, Bonni A, Zigmond MJ, Lin MZ, Juo P, Hu LS, Anderson MJ, Arden KC, Blenis J, Greenberg ME (1999) Akt promotes cell survival by phosphorylating and inhibiting a forkhead transcription factor. *Cell* 96: 857–868
- Byles V, Covarrubias AJ, Ben-Sahra I, Lamming DW, Sabatini DM, Manning BD, Horng T (2013) The TSC-mTOR pathway regulates macrophage polarization. *Nat Commun* 4: 2834
- Candiracci J, Migeot V, Chionh YH, Bauer F, Brochier T, Russell B, Shiozaki K, Dedon P, Hermand D (2019) Reciprocal regulation of TORC signaling and tRNA modifications by elongator enforces nutrient-dependent cell fate. *Sci Adv* 5: eaav0184
- Cassado AA, D'Império Lima MR, Bortoluci KR (2015) Revisiting mouse peritoneal macrophages: Heterogeneity, development, and function. *Front Immunol* 6: 225
- Cruz-Gordillo P, Honeywell ME, Harper NW, Leete T, Lee MJ (2020) ELP-dependent expression of MCL1 promotes resistance to EGFR inhibition in triple-negative breast cancer cells. *Sci Signal* 13: eabb9820
- Delaunay S, Rapino F, Tharun L, Zhou Z, Heukamp L, Termathe M, Shostak K, Klevernic I, Florin A, Desmecht H et al (2016) Elp3 links tRNA modification to IRES-dependent translation of LEF1 to sustain metastasis in breast cancer. *J Exp Med* 213: 2503–2523
- Dewez M, Bauer F, Dieu M, Hermand D (2008) The conserved wobble uridine tRNA thiolase Ctu1–Ctu2 is required to maintain genome integrity. *Proc Natl Acad Sci U S A* 105: 5459–5464
- Düvel K, Yecies JL, Menon S, Raman P, Lipovsky AI, Souza AL, Triantafellow E, Ma Q, Gorski R, Cleaver S et al (2010) Activation of a metabolic gene regulatory network downstream of mTOR complex 1. *Mol Cell* 39: 171–183
- El Yacoubi B, Bailly M, De Crécy-Lagard V (2012) Biosynthesis and function of posttranscriptional modifications of transfer RNAs. *Annu Rev Genet* 46: 69–95
- Erben U, Loddenkemper C, Doerfel K, Spieckermann S, Haller D, Heimesaat MM, Zeitz M, Siegmund B, Kühl AA (2014) A guide to histomorphological evaluation of intestinal inflammation in mouse models. *Int J Clin Exp Pathol* 7: 4557–4576
- Festuccia WT, Pouliot P, Bakan I, Sabatini DM, Laplante M (2014) Myeloid-specific rictor deletion induces M1 macrophage polarization and potentiates *in vivo* pro-inflammatory response to lipopolysaccharide. *PLoS One* 9: e95432
- Galdiero MR, Garlanda C, Jaillon S, Marone G, Mantovani A (2013) Tumor associated macrophages and neutrophils in tumor progression. *J Cell Physiol* 228: 1404–1412
- Gordon S, Martinez FO (2010) Alternative activation of macrophages: mechanism and functions. *Immunity* 32: 593–604
- Hallowell RW, Collins SL, Craig JM, Zhang Y, Oh M, Illei PB, Chan-Li Y, Vigeland CL, Mitzner W, Scott AL et al (2017) mTORC2 signalling regulates M2 macrophage differentiation in response to helminth infection and adaptive thermogenesis. *Nat Commun* 8: 14208
- Hendriks MMWB, Smit S, Akkermans WLMW, Reijmers TH, Eilers PHC, Hoefsloot HCJ, Rubingh CM, De Koster CG, Aerts JM, Smilde AK (2007) How to distinguish healthy from diseased? Classification strategy for mass spectrometry-based clinical proteomics. *Proteomics* 7: 3672–3680
- Hou J, Schindler U, Henzel WJ, Ho TC, Brousseau M, McKnight SL (1994) An interleukin-4-induced transcription factor: IL-4 stat. *Science* 265: 1701–1706
- Howell JJ, Manning BD (2011) mTOR couples cellular nutrient sensing to organismal metabolic homeostasis. *Trends Endocrinol Metab* 22: 94–102
- Huang SCC, Smith AM, Everts B, Colonna M, Pearce EL, Schilling JD, Pearce EJ (2016) Metabolic reprogramming mediated by the mTORC2-IRF4 signaling axis is essential for macrophage alternative activation. *Immunity* 45: 817–830
- Jenkins SJ, Ruckerl D, Cook PC, Jones LH, Finkelman FD, van Rooijen N, MacDonald AS, Allen JE (2011) Local macrophage proliferation, rather than recruitment from the blood, is a signature of TH2 inflammation. *Science* 332: 1284–1288
- Jha AK, Huang SCC, Sergushichev A, Lampropoulou V, Ivanova Y, Loginicheva E, Chmielewski K, Stewart KM, Ashall J, Everts B et al (2015) Network integration of parallel metabolic and transcriptional data reveals metabolic modules that regulate macrophage polarization. *Immunity* 42: 419–430
- Kim JH, Lee E, Friedline RH, Suk S, Jung DY, Dagdeviren S, Hu X, Inashima K, Noh HL, Kwon JY et al (2018) Endoplasmic reticulum chaperone GRP78 regulates macrophage function and insulin resistance in diet-induced obesity. *FASEB J* 32: 2292–2304
- Ladang A, Rapino F, Heukamp LC, Tharun L, Shostak K, Hermand D, Delaunay S, Klevernic I, Jiang Z, Jacques N et al (2015) Elp3 drives Wnt-dependent

- tumor initiation and regeneration in the intestine. *J Exp Med* 212: 2057–2075
- Laguesse S, Creppe C, Nedialkova DD, Prévot PP, Borgs L, Huysseune S, Franco B, Duysens G, Krusy N, Lee G et al (2015) A dynamic unfolded protein response contributes to the control of cortical neurogenesis. *Dev Cell* 35: 553–567
- Laplante M, Sabatini DM (2012) mTOR signaling in growth control and disease. *Cell* 149: 274–293
- Lemaitre P, Bai Q, Legrand C, Chariot A, Close P, Bureau F, Desmet CJ (2021) Loss of the transfer RNA wobble uridine-modifying enzyme Elp3 delays T cell cycle entry and impairs T follicular helper cell responses through deregulation of Atf4. *J Immunol* 206: 1077–1087
- Liu GY, Sabatini DM (2020) mTOR at the nexus of nutrition, growth, ageing and disease. *Nat Rev Mol Cell Biol* 21: 183–203
- Liu PS, Wang H, Li X, Chao T, Teav T, Christen S, Di Conza G, Cheng WC, Chou CH, Vavakova M et al (2017) A-ketoglutarate orchestrates macrophage activation through metabolic and epigenetic reprogramming. *Nat Immunol* 18: 985–994
- Lumeng CN, Bodzin JL, Saltiel AR (2007) Obesity induces a phenotypic switch in adipose tissue macrophage polarization. *J Clin Invest* 117: 175–184
- Murray PJ (2017) Macrophage polarization. *Annu Rev Physiol* 79: 541–566
- Murray PJ, Wynn TA (2011) Protective and pathogenic functions of macrophage subsets. *Nat Rev Immunol* 11: 723–737
- Murray PJ, Allen JE, Biswas SK, Fisher EA, Gilroy DW, Goerdt S, Gordon S, Hamilton JA, Ivashkiv LB, Lawrence T et al (2014) Macrophage activation and polarization: Nomenclature and experimental guidelines. *Immunity* 41: 14–20
- Nagai MH, Xavier VPS, Gutiyama LM, Machado CF, Reis AH, Donnard ER, Galante PAF, Abreu JG, Festuccia WT, Malnic B (2020) Depletion of Ric-8B leads to reduced mTORC2 activity. *PLoS Genet* 16: e1008255
- Nedialkova DD, Leidel SA (2015) Optimization of codon translation rates via tRNA modifications maintains proteome integrity. *Cell* 161: 1606–1618
- O'Neill LAJ (2016) A metabolic roadblock in inflammatory macrophages. *Cell Rep* 17: 625–626
- Pulendran B, Artis D (2012) New paradigms in type 2 immunity. *Science* 337: 431–435
- Rapino F, Delaunay S, Zhou Z, Chariot A, Close P (2017) tRNA modification: is cancer having a wobble? *Trends Cancer* 3: 249–252
- Rapino F, Delaunay S, Rambow F, Zhou Z, Tharun L, De Tullio P, Sin O, Shostak K, Schmitz S, Piepers J et al (2018) Codon-specific translation reprogramming promotes resistance to targeted therapy. *Nature* 558: 605–609
- Rodríguez-Prados J-C, Través PG, Cuenca J, Rico D, Aragónés J, Martín-Sanz P, Cascante M, Boscá L (2010) Substrate fate in activated macrophages: a comparison between innate, classic, and alternative activation. *J Immunol* 185: 605–614
- Rosu A, El Hachem N, Rapino F, Rouault-Pierre K, Jorssen J, Somja J, Ramery E, Thiry M, Nguyen L, Jacquemyn M et al (2021) Loss of tRNA-modifying enzyme Elp3 activates a p53-dependent antitumor checkpoint in hematopoiesis. *J Exp Med* 218: e20200662
- Rubio RM, Depledge DP, Bianco C, Thompson L, Mohr I (2018) RNA m⁶a modification enzymes shape innate responses to DNA by regulating interferon β . *Genes Dev* 32: 1472–1484
- Ryan DG, O'Neill LAJ (2020) Krebs cycle reborn in macrophage immunometabolism. *Annu Rev Immunol* 38: 289–313
- Saha S, Shalova IN, Biswas SK (2017) Metabolic regulation of macrophage phenotype and function. *Immunol Rev* 280: 102–111
- Shulman Z, Stern-Ginossar N (2020) The RNA modification N⁶-methyladenosine as a novel regulator of the immune system. *Nat Immunol* 21: 501–512
- Stein M, Keshav S, Harris N, Gordon S (1992) Interleukin 4 potently enhances murine macrophage mannose receptor activity: a marker of alternative immunologic macrophage activation. *J Exp Med* 176: 287–292
- Su LK, Kinzler KW, Vogelstein B, Preisinger AC, Moser AR, Luongo C, Gould KA, Dove WF (1992) Multiple intestinal neoplasia caused by a mutation in the murine homolog of the APC gene. *Science* 256: 668–670
- Tavares JF, Davis NK, Poim A, Reis A, Kellner S, Sousa I, Soares AR, Moura GMR, Dedon PC, Santos M (2020) tRNA-modifying enzyme mutations induce codon-specific mistranslation and protein aggregation in yeast. *RNA Biol* 18: 563–575
- Vats D, Mukundan L, Odegaard JI, Zhang L, Smith KL, Morel CR, Greaves DR, Murray PJ, Chawla A (2006) Oxidative metabolism and PGC-1 β attenuate macrophage-mediated inflammation. *Cell Metab* 4: 13–24
- Wang J-M, Chao J-R, Chen W, Kuo M-L, Yen J-J-Y, Yang-Yen H-F (1999) The antiapoptotic gene mcl-1 is up-regulated by the phosphatidylinositol 3-kinase/Akt signaling pathway through a transcription factor complex containing CREB. *Mol Cell Biol* 19: 6195–6206
- Winkler R, Gillis E, Lasman L, Safra M, Geula S, Soyris C, Nachshon A, Tai-Schmiedel J, Friedman N, Le-Trilling VTK et al (2019) M⁶a modification controls the innate immune response to infection by targeting type I interferons. *Nat Immunol* 20: 173–182
- Xia J, Sinelnikov IV, Han B, Wishart DS (2015) MetaboAnalyst 3.0-making metabolomics more meaningful. *Nucleic Acids Res* 43: W251–W257
- Yano T, Ferlito M, Aponte A, Kuno A, Miura T, Murphy E, Steenberger C (2014) Pivotal role of mTORC2 and involvement of ribosomal protein S6 in cardioprotective signaling. *Circ Res* 114: 1268–1280



License: This is an open access article under the terms of the [Creative Commons Attribution](#) License, which permits use, distribution and reproduction in any medium, provided the original work is properly cited.